https://doi.org/10.5194/essd-2020-244
Preprint. Discussion started: 23 September 2020

A novel hydrographic gridded data set for the Northern Antarctic Peninsula

Tiago S. Dotto[1], Mauricio M. Mata[1,2], Rodrigo Kerr[1,2], Carlos A. E. Garcia[1,2]

[1]Laboratório de Estudos dos Oceanos e Clima, Instituto de Oceanografia, Universidade Federal do Rio Grande-FURG, Brazil
[2]Programa de Pós-Graduação em Oceanologia, Instituto de Oceanografia, Universidade Federal do Rio Grande-FURG, Brazil

Correspondence to: Tiago S. Dotto (tiagosdotto@gmail.com)

Abstract. The Northern Antarctic Peninsula (NAP) is a highly dynamic transitional zone between the subpolar-polar and oceanic-coastal environments, and it is located in an area affected by intense climate change, including intensification and spatial shifts of the westerlies as well as atmospheric and oceanic warming. In the NAP area, the water masses originate mainly from the Bellingshausen and Weddell Seas, which create a marked regional dichotomic thermohaline characteristic. Although the NAP area has relatively easy access when compared to other Southern Ocean environments, our understanding of the water masses distribution and the dynamical processes affecting the variability of the region is still limited. That limitation is closely linked to the sparse data coverage, as commonly is the case in most of the Southern Ocean environments. This work provides a novel three-dimensional high-resolution hydrographic gridded data set for the NAP, namely the GOAL gridded product. Hydrographic measurements from 2003-2019 have been optimally interpolated to produce maps of conservative temperature, absolute salinity, neutral density and dissolved oxygen at ~10 km spatial resolution and 114 depth levels. The water masses and oceanographic features in this regional gridded product are more accurate than other climatologies and state estimate products currently available. The data sets are available in netCDF format at https://www.goal.furg.br/producao-cientifica/supplements/203-goal-gridded-nap and at https://doi.org/10.5281/zenodo.3989548 (Dotto et al., 2020). The novel GOAL gridded product and comprehensive data sets presented here are a valuable tool to be used in studies addressing climatological changes in the unique NAP region since they provide accurate initial conditions for ocean models and improve the early 21st-century ocean mean-summer-state representation for that area.

1 Introduction

The Northern Antarctic Peninsula (NAP; Kerr et al., 2018a) encompasses the Bransfield and Gerlache Straits, the northwestern Weddell Sea, the southernmost Drake Passage and the northern end of the West Antarctic Peninsula environments (Fig. 1). The NAP is a sensitive region to climate changes because it is located under the influence of the westerly winds, which are prone to current intensification and poleward migration (Marshall, 2003; Swart and Fyfe, 2012; Lin et al., 2018). The region also receives considerable freshwater input from the melting of glaciers from the Antarctic Peninsula (Cook et al., 2016; Rignot et al., 2019). Moreover, the NAP has been showing significant alterations in its water masses physico-

https://doi.org/10.5194/essd-2020-244
Preprint. Discussion started: 23 September 2020

chemical properties, such as warming, freshening, and acidification (Gordon et al., 2000; Meredith and King, 2005; Hellmer et al., 2011; Dotto et al., 2016; Kerr et al., 2018b; Lencina Avila et al., 2018; Ruiz Barlett et al., 2018), a decline in sea ice extension and shortening of sea ice cover season (Stammerjohn et al., 2008; Turner et al., 2013), as well as in its marine ecosystem (Moline et al., 2004; Montes-Hugo et al., 2009; Mendes et al., 2013).

Water masses with different properties and origins reach the NAP and mix to form the dense water masses that sink and fill the deep basins of the Bransfield Strait (Gordon et al., 2000; Dotto et al., 2016; Huneke et al., 2016; van Caspel et al., 2018). High Salinity Shelf Water (HSSW) and Low Salinity Shelf Water (LSSW) from the Weddell Sea enter the NAP from the east, mainly contouring the Antarctic Peninsula (von Gyldenfeldt et al. 2002; Heywood et al., 2004; Thompson et al., 2009; Collares et al., 2018), and then sinking along the slope and at the Bransfield Strait's several canyons (van Caspel et al., 2018). A branch carrying modified HSSW flows southwestward along the continental shelf to the west of the Antarctic Peninsula and reaches as far as the Gerlache Strait (Sangrà et al. 2017; Kerr et al., 2018b). Conversely, modified Circumpolar Deep Water (mCDW) from the Bellingshausen Sea – a relatively warm, salty, nutrient-rich and deoxygenated water mass derived from the intermediate waters of the Antarctic Circumpolar Current (ACC) and modified over the western Antarctic Peninsula continental shelf – enters the NAP mainly through the Bransfield Strait western basin (Smith et al., 1999; Ruiz Barlett et al., 2018), flowing northeastward along the South Shetland Islands slope as the Bransfield Current (Sangrà et al., 2011). The mCDW also intrudes into the Bransfield Strait from the southern Drake Passage between King George and Elephant islands (López et al., 1999; Gordon et al., 2000). Therefore, a cyclonic circulation pattern is created within the Bransfield Strait from currents of completely different origins defining a strong transitional signature for that whole area (García et al., 2002). Two main fronts are observed in this region: the Bransfield Front and the Peninsula Front (Sangrà et al. 2011). The Bransfield Front is the mid-depth front separating the warm waters flowing along with the Bransfield Current and the cold waters within the deep basins of the Bransfield Strait. The Peninsula Front separates, in shallow depths, the cold waters from Weddell influence and the Bransfield Strait waters. In the Gerlache Strait, mCDW from the Bellingshausen Sea also intrudes from the south and through the gaps near the Anvers Island (Smith et al., 1999; García et al., 2002; Torres Parra et al., 2020). The mCDW interacts with the HSSW-sourced waters, and a relatively colder mixture leaves the Gerlache Strait towards the western basin of the Bransfield Strait (Niiler et al., 1991; Zhou et al., 2002; Savidge and Amft, 2009).

For the past fifty years at least, the deep waters of the Bransfield Strait have shown significant trends of freshening and lightening, with impacts on the volume of these regional dense waters (Azaneu et al., 2013; Dotto et al., 2016; Ruiz Barlett et al., 2018). Considering that these waters are formed by a parcel of ~60-80% of HSSW+LSSW (Gordon et al., 2000; Dotto et al., 2016), the freshening signal may be driven by modification of the water masses sourced in the Weddell Sea continental shelf (van Caspel et al., 2015, 2018), possibly due to the melting of ice shelves and glaciers in the Antarctic Peninsula (Cook et al., 2016; Rignot et al., 2019). In addition, the decreasing of the sea ice concentration and the shortening of the sea ice season in the NAP (Stammerjohn et al., 2008; Turner et al., 2013) may also play a role in the freshening trend due to a reduction of the salt flux into these shelf waters (Hellmer et al., 2011).

https://doi.org/10.5194/essd-2020-244
Preprint. Discussion started: 23 September 2020

A better understanding of the NAP oceanic and shelf circulation, as well as the connection to the Weddell and Bellingshausen Seas, is important to help to assess the evolution and impacts of the ocean on the ice shelves and glaciers melting downstream (Cook et al., 2016; Rignot et al., 2019). Currently, the overall change in the glaciers' area is relatively small in the Bransfield and Gerlache straits compared to the adjacent Bellingshausen coastline, which is under the influence of warmer waters. However, changes in proportions of the inflowing water masses could potentially lead these regions to a Bellingshausen Sea-like scenario, where warmer oceanic conditions shape the local glacier fronts behaviour and higher melting rates are observed (Cook et al., 2016). Ruiz Barlett et al. (2018) suggest that persistent northerly and westerly wind conditions, concurrent with La Niña and positive phases of the Southern Annular Mode (SAM), are favourable drivers for mCDW inflow into the NAP. These warm inflows are likely facilitated by the poleward displacements of the oceanic fronts associated with the ACC during La Niña events (Loeb et al., 2009). Additionally, positive SAM may restrict the connections between the Weddell Sea and the Bransfield Strait (Renner et al., 2012), with the potential of reducing the inflow of cold waters into the NAP (Dotto et al., 2016). The ongoing changes in the Southern Hemisphere wind pattern, i.e. poleward and intensification associated with positive trends in the SAM, and an increase in the energetics of the ACC (Meredith and Hogg, 2006; Hogg et al., 2015) could then lead to higher mCDW inflow into the NAP by advection (e.g., Ruiz Barlett et al., 2018) and/or eddies shed by the ACC (Martinson and McKee, 2012; Couto et al., 2017). Although the strengthening of winds tends to increase the inflow of warm waters toward the west Antarctic Peninsula continental shelf, it does not necessarily mean higher ice shelf basal melting (except for the shallower ice shelves). Conversely, models suggest a reduction of sea ice concentration associated with an enhancement of the upper ocean heat fluxes (Dinniman et al., 2012). In the NAP, mixing rate measurements are scarce, hampering the understanding of how heat fluxes in the upper and deeper ocean will respond to the future wind changes in the region. In addition, there is still a lack of information regarding the water masses fluxes and mixing between the Powell Basin in the Weddell Sea and the Bransfield Strait (Thompson et al., 2009; Azaneu et al., 2017), which would help to increase our understanding of the complex coastal Antarctic system.

In this context, forecasts of the evolution of the dynamics of these regional seas and their interconnections in future climate change scenarios are needed. In general, in situ measurements in the Southern Ocean are scarce in space and time due to logistical constraints. Moreover, that scarceness impacts a proper understanding of the oceanographic processes and their interactions with the atmosphere and cryosphere, which requires robust and long-term Southern Ocean observing systems to provide high-quality measurements of the different compartments (Meredith et al., 2013; Newman et al., 2019). Hence, high-resolution regional models are needed to integrate these data and to simulate future scenarios. In this sense, quality-controlled gridded products to feed these models are important to properly create the initial conditions, in terms of the 3D structure of the water masses, which are needed to capture the main oceanographic and glaciological interactions and, consequently, their future evolution.

Since 2003, the Brazilian High Latitude Oceanography Group (GOAL; Mata et al., 2018) has been conducting research cruises on a quasi-annual basis in the NAP area during summer periods. Most of the efforts have focused on the Bransfield and Gerlache straits, due to their relatively easier access, logistics and favourable meteo-oceanographic conditions.

https://doi.org/10.5194/essd-2020-244
Preprint. Discussion started: 23 September 2020

Here, we present a hydrographic gridded product comprising the robust high-resolution and quasi-synoptic measurements made during the GOAL cruises conducted between 2003 to 2019 in the NAP. This gridded product can be used for several applications, including input data for ocean and climate models initialization/assessment and ocean reanalysis evaluation, as well as to produce and reconstruct biogeochemical properties. Finally, the GOAL gridded product represents the ocean mean-summer-state for the NAP in the early 21st-century.

2 Hydrographic cruises, data sampling and ancillary data set

Six main projects were carried out by the GOAL from 2003 to 2019 in the NAP area: REDE-1 (Mata and Garcia, 2016a,b,c), SOS-CLIMATE (Mata and Garcia, 2016d,e,f), POLARCANION/PRO-OASIS (Mata and Kerr, 2016a,b,c), and NAUTILUS/INTERBIOTA (Kerr et al., 2018a and references therein; Table 1). Most of the cruises covered the Bransfield and Gerlache straits, followed by the Bellingshausen Sea during the NAUTILUS/INTERBIOTA projects and the northwestern Weddell Sea during the SOS-CLIMATE project (Table 1 and Fig. 2). The data sampling took place only in austral summer conditions, most of the time in February (~65%), followed by January (~27%) and March (~8%). The number of hydrographic profiles collected annually by the GOAL during the period 2003-2019 ranged from a minimum of 28 in 2011 to the maximum of 108 in 2013, with an average of 64 hydrographic stations per year in the NAP (Fig. 3a).

The data sampling was performed by a Conductivity, Temperature, and Depth (CTD) Sea-Bird Electronics® (SBE) 911plus system equipped with doubled sensors of temperature (SBE 3plus), conductivity (SBE 4C) and dissolved oxygen (DO; SBE 43), except in a few stations in the 2005 cruise. However, this had virtually no influence on the final gridded data set because the vertical resolution is coarser than the CTD sampling and the data is merged in the interpolation process with the remaining dataset from different years. The CTD was integrated with an SBE 32 Carousel Water Sampler. The CTD data were pre-processed onboard according to common standards (e.g., data conversion, wild points flagging, conductivity thermal mass correction, pressure reversal and minimum velocity flagging, etc.), following the manufacturer's manual, and using Sea-Bird Data Processing software routines. Data were averaged onto 1 dbar pressure intervals and saved for post-processing on land.

Spurious data from all variables used (i.e., temperature, salinity and DO) that remained after the pre-processing were manually flagged and removed on land. This last step removed less than ~0.50% of temperature data and less than ~1% of salinity data. The CTD's DO was corrected for drifts using Winkler titration (Carpenter, 1965; Culberson et al., 1991) of water samples carried out on board, except in the 2011 and 2013 cruises. In 2011, the mean DO profile showed a mean overestimation of ~1 mL L^{-1}, compared to the mean profile of all other years. Nevertheless, the mean absolute difference between the mean profile of all years considering 2011 and the mean profile excluding 2011 is only 0.02 mL L^{-1}, which is of similar magnitude to when excluding any other year. In 2013, the DO sensor-measured was in good agreement in terms of vertical structure and magnitude compared to years corrected for Winkler, showing a mean underestimation of ~–0.12 mL L^{-1}. Thus, we decided to include 2011 and 2013 DO data in our gridded product. After identifying the best profiles of DO to be used in this work, spurious data that remained were removed and represented ~6% of the remained data set. The mean absolute difference between the doubled sensors were ~0.001°C and ~0.003 for temperature and salinity, respectively, considering all cruises. For the DO sensors, the mean absolute difference was ~0.09 mL L^{-1}, after removing profiles from sensors that presented a visible offset. Finally, conservative temperature (Θ), absolute salinity (S_A) and neutral density (γ^n) were computed (Jackett and McDougall, 1997; McDougall and Barker, 2011). See Table 1 for more information about the sampled region, dates and variables measured in each cruise.

We have done a reasonableness check with individual GOAL data to verify if the gridded products can represent the expected and accepted values. We also investigated how GOAL gridded product can be compared with an independent dataset. Therefore, historical hydrographic data were downloaded from the US National Oceanographic Data Centre (NODC; https://www.nodc.noaa.gov/OC5/SELECT/dbsearch/dbsearch.html). We selected data restricted to the NAP (within the area 50°-68°W and 60°-66°S) for the period 2003-2019 between January and March. Only data flagged as "good" were considered, and spurious data that remained were manually removed. Summer-averaged temperature and salinity for the period 2005-2017 from the World Ocean Atlas 2018 (WOA; https://www.nodc.noaa.gov/OC5/woa18/woa18data.html; Locarnini et al., 2018; Zweng et al., 2018) was also used to compare with the GOAL gridded product (Sect. 3). WOA has a spatial resolution of 1/4° and 102 vertical levels. DO is available only in coarser resolution, thus it is not used here. The Commonwealth Scientific and Industrial Research Organisation (CSIRO) Atlas of Regional Seas (CARS; http://www.marine.csiro.au/~dunn/cars2009/; Ridgway et al., 2002) was also used in the same way. CARS has a spatial resolution of 1/2°, 79 vertical levels and it comprises gridded fields of the mean ocean temperature, salinity and DO. The summer season mean conditions are estimated from the annual and semi-annual coefficients distributed with the climatological fields; however, these coefficients are limited to the mid- and upper-levels. Finally, the Southern Ocean State Estimate (SOSE; http://sose.ucsd.edu/; Mazloff et al., 2010), coupled with biogeochemical-sea ice-ocean state estimate (Verdy and Mazloff, 2017), was used to compare with our regional gridded product. February outputs of the runs called iterations 106 and 133 were averaged to produce a mean state for the period 2008-2018 (the biogeochemical outputs are not available prior to this period). Potential temperature, practical salinity and DO were selected with a spatial resolution of 1/6° and 52 vertical levels. Θ and S_A were then computed for all data sets prior to the assessment.

3 Methods

Before gridding, each GOAL CTD profile was linearly interpolated onto 114 depth levels, ranging from 5 m to 4450 m (Table 2). The depth spacing ranges from 5 m in the upper 50 m to 75 m below 2200 m depth, which correspond mostly to the oceanic regions outside the straits. The levels were arbitrarily selected. After this vertical interpolation, the number of samples per depth ranged from >800 in the upper 200 m, decreasing to <50 in depths deeper than 2200 m (Fig. 3b). The number of samples of DO per depth is smaller than those of Θ, S_A and γ^n. That is a consequence of DO not being measured in some years and also more DO data were excluded in the quality control or during the pre- and post-processing stages previously mentioned than Θ, S_A and γ^n (Table 1).

The scattered data were objectively interpolated onto a regular grid of ~10 km resolution. The grid spacing is 0.09° along latitudes and 0.2° along longitudes (i.e., 0.09° latitude × 0.09°/cos(63°S) longitude, where 63°S is the mean latitude of our domain). The limits of the domain are 60°S to 66°S and 50°W to 66°W. Bathymetry and land masks were applied using the 1 arc-minute ETOPO1 Ice Surface data set (https://www.ngdc.noaa.gov/mgg/global/) interpolated onto a grid of same resolution.

The objective interpolation uses scattered observations to generate a regular gridded and smoothed version of the original data field analysed (Bretherton et al., 1976; Thomson and Emery, 2014). The method is based on the Gauss-Markov theorem, which consists of an application of linear estimation techniques for interpolating data from the multiple surveys combined. While this improves the spatial coverage, it also smooths out the temporal and spatial variability, resulting in a pattern that is more representative of the large-scale mean state rather than of a specific cruise. Figure 4 shows the number of hydrographic stations per grid cell per depth (only Θ is shown for display purposes). Most of the grid cells are occupied by at least two stations. However, some grid cells within the Bransfield Strait present more than 10 stations each. The interpolation of each grid point is affected by the neighbouring data that fall within the smoothing lengthscales (or radius of influence) and the relative error chosen a priori. The interpolation method also assumes a weight to sum all observations within a specific smoothing lengthscale. The weight is a function of the distance to the grid point and the location of the observation only. Because the objective interpolation fits a Gaussian function, the nearest neighbours have higher weight than the data located closer to the edge of the radius of influence. A series of tests were made to find the appropriate smoothing lengthscale and the a priori relative error in order to find a balance between smoothness and feature representativeness. The final smoothing lengthscale (i.e. the radius of influence of the interpolation) chosen was 0.8° in latitude and longitude, and the a priori relative error allowed was set to 0.1 for the objective interpolation algorithm. The same constants were set for all depth levels and all variables. Regions where the mapping relative error was higher than 0.5 were excluded. The matrices of relative errors are provided together with the gridded variables, so the user can choose the relative error level to work with (between 0 and 0.5). The representativeness of the interpolated maps decreases as the number of measurements being used reduces. This is reflected in higher relative errors, such as seen closer to the (i) borders of the domain, (ii) regions where the gaps between data are large, and (iii) at deeper levels (Fig. 5).

4 Results and discussion

4.1 Reasonableness check of the gridded product and comparison with an independent data set

4.1.1 Reasonableness check

The term reasonableness check is used here to ensure that the gridded data set meets the expected range, type or value based on its individual measurements. We want to examine how reasonable the GOAL gridded product can represent the CTD

https://doi.org/10.5194/essd-2020-244
Preprint. Discussion started: 23 September 2020

profiles closer than ~6 km of each grid point. Although the data sets are not independent, this comparison shows how well the interpolation captured the real data set's magnitude, structure and spatial variability. Qualitatively, the gridded product and the profiles have a good agreement for the hydrographic parameters. For instance, considering Θ at 500 m depth, the highest discrepancies are observed close to the edge of the domain (e.g., southern Drake Passage), near to meanders and fronts (e.g., northwestern Weddell Sea and within the Bransfield Strait), as well as associated with areas of steep continental slope (Fig. 6a). The differences between the gridded product and the profiles are larger in the upper 500 m, where higher interannual variability is expected (Fig. 6b). The average difference along the water column is 0.01˚C, which is of same magnitude as at 500 m. Taking into account all data from the gridded product and only the grid points which have data profiles within a ~6 km radius shown in Fig. 6a, 68% of the data points fall within the difference range of ±0.2˚C (Fig. 6c). We note that the NAP has a considerable Θ interannual variability (Mendes et al., 2013; Gonçalves Araújo et al., 2015; Dotto et al., 2016; Ruiz Barlett et al., 2018) that is smoothed out in the interpolation process and can impact the observed differences. Overall, the mean squared error between the gridded product and the profiles is higher in the upper 500 m depth (i.e. > 0.05˚C^2 and < 0.2˚C^2) and decreases to < 0.05˚C^2 below that level (Fig. 6d).

A good agreement between the GOAL gridded product and the profiles is also observed for S_A, except in southern Drake Passage, and regions associated with meanders and fronts, where the ocean variability is higher and the interpolation smooths out most of these small-scale processes (Fig. 7a). The differences over the water column are higher in the upper levels due to the interannual variability, and smaller towards the deep ocean (Fig. 7b). The average differences, however, lie on the third decimal place. About 72% of the differences between the gridded product the profiles are between ±0.04 g kg^{-1} (Fig. 7c). The mean squared error is smaller than 0.02 (g kg^{-1})^2 in most of the water column (Fig. 7d). The errors show a steep decrease function in the upper 200 m, whereas below that level, the errors are found beyond the third decimal place.

The GOAL gridded product shows relatively higher differences related to DO data (Fig. 8a), which is a non-conservative property. The largest differences are observed near fronts and within the Bransfield Strait, where the DO variability is higher. Along the water column, the spreading of the differences between the gridded product and the profiles are relatively high, reaching differences of ±0.5 mL L^{-1} between 1000-1500 m depth (Fig. 8b). Nevertheless, the water column mean difference lies on the third decimal for DO as well. About 65% of the DO differences fall within the range ±0.2 mL L^{-1} (Fig. 8c). The mean squared error is above 0.04 (mL L^{-1})^2 in the upper 1500 m, decreasing close to zero below 2000 m depth (Fig. 8d).

4.1.2 Comparisons with independent profiles

A comparison between GOAL gridded product and NODC profiles, closest ~6 km, are presented here. Note that the sampling dates of the NODC data are not necessarily the same of GOAL, and thus, differences in magnitude between the properties compared might occur. Most of the NODC profiles are located in areas outside the Bransfield and Gerlache straits (Fig. 9a). The inner Bransfield Strait, Gerlache Strait and the deep basins, such as Weddell Sea and Powell Basin, are the

https://doi.org/10.5194/essd-2020-244
Preprint. Discussion started: 23 September 2020

regions where the difference between Θ, S_A and DO from the GOAL gridded product and the NODC are smallest (Fig. 9a,c,e). Conversely, Θ, S_A and DO differences are relatively higher close to the Elephant Island, a region where the Antarctic Circumpolar Current (ACC) flows along the slope (Fig. 9a,c,e). Regions near fronts (e.g., northwestern Weddell Sea and the Antarctic Slope Front; Heywood et al., 2004) also show high differences between the data sets because the GOAL gridded product tends to smooth out those features. Larger differences are also observed at the surface, likely due to the higher temporal variability observed in the region (Fig. 9b,d,f). Nevertheless, the averaged differences along the water column between the GOAL gridded product and the NODC data are –0.15°C, –0.02 g kg^{-1} and –0.09 mL L^{-1}.

4.2 Representation of the main hydrographic features in the NAP

The GOAL gridded product represents qualitatively well the surface thermal dichotomic regime of waters of the NAP: a warm variety with Bellingshausen Sea and ACC influence, and a cold Weddell Sea-sourced water (Fig. 10a). A surface thermal front splits these two regimes near the Antarctic Peninsula, likely depicting the Peninsula Front (López et al., 1999; Sangrà et al., 2011). In the surface, the Weddell Sea-sourced waters are saltier and denser compared to the warm waters to the west of the NAP (Fig. 10a-c). Thus, the Peninsula Front seems to be baroclinic (Sangrà et al., 2011). The DO is relatively supersaturated everywhere, with higher concentrations found close to the James Ross Island and the northern end of the Gerlache Strait (Fig. 10d). These regions are generally associated with high primary productivity, which could explain the relatively higher values of DO (Mendes et al., 2012; Detoni et al., 2015; Costa et al., 2020).

In deeper layers, the dichotomic regime of the NAP is still evident (Fig. 11a), reflecting the presence of warm and salty waters associated with the mCDW to the west of the NAP and the Warm Deep Water (a warm, salty and poor-oxygenated intermediate water mass presented in the Weddell Sea and derived from the mixing between CDW and Winter Water) within the offshore zone of the Weddell Sea and Powell Basin (Fig. 11a,b). Intrusions of mCDW are observed in the Bellingshausen Sea, reaching the Gerlache Strait and the western basin of the Bransfield Strait. After entering the Bransfield Strait, a warm signal follows the slope of the South Shetland Islands, suggesting the presence of the narrow Bransfield Current (Fig. 11a; Niiler et al., 1991; López et al., 1999; Zhou et al., 2006; Sangrà et al., 2011). Conversely, at the Weddell Sea continental shelf and central and eastern Bransfield Strait basins, the waters are colder and fresher (Fig. 11a,b). The γ^n distribution shows slightly denser waters contouring the Antarctic Peninsula shelf break (Fig. 11c), which is likely associated with the intrusions of water from the Weddell Sea (Heywood et al., 2004). The water masses in the Bransfield Strait central basin are slightly denser than in the eastern basin, suggesting a different origin of these waters (Gordon et al., 2000; van Caspel et al., 2018). Following Θ distribution, DO is higher on the Weddell Sea continental shelf and within the Bransfield Strait, whereas the lower values are observed associated with the older water masses mCDW and the Warm Deep Water (Fig. 11d). Although the routes of mCDW inflow are relatively well known, few studies focused on the periodicity of these inflows into the NAP (e.g., Ruiz Barlett et al., 2018) or on the fast response of these inflows associated with the wind forcing (e.g., McKee and Martinson, 2020). The comprehension of these mechanisms is important to better resolve the heat and salt fluxes into the NAP.

https://doi.org/10.5194/essd-2020-244
Preprint. Discussion started: 23 September 2020

The bottom properties show the cold-fresh regime in the northwestern Weddell Sea and the Bransfield Strait, whereas a warm-salty regime can be seen in oceanic areas southwestern of the NAP (Fig. 12a,b). The Gerlache Strait and the west basin of the Bransfield Strait have intermediate regimes of Θ and S_A compared to those areas previously mentioned. The Bransfield Strait central basin has the highest γ^n values compared to the surroundings (Fig. 12c). This distinction could be associated with the higher contribution of HSSW to the central basin (Gordon et al., 2000; Dotto et al., 2016). These dense waters that flood the central basin deep levels seem to follow the shortcuts of the canyons that cut across the Antarctic Peninsula continental shelf in the Bransfield Strait. Associated with the cold waters, the DO is high on the Weddell Sea continental shelf and along the route of these flows toward the northern Gerlache Strait (Fig. 12d). When these cold and dense waters sink into the central Bransfield Strait basin, they carry high concentration of oxygen (where depths are >1000 m). The high DO in that deep region indicates a fast route of Weddell Sea shelf waters and hence a small residence time (van Caspel et al., 2015, 2018).

To exemplify the representation of the water column in the NAP, we selected five sections crossing the Bransfield Strait (Fig. 13 and 14). To the south, along the section between Livingston Island and the Antarctic Peninsula, relatively warmer conditions are observed from the upper ocean to the bottom layers (Fig. 13a). Also, mCDW is observed between 62.7-62.8°S, where the isotherms are sharply tilted towards the South Shetland Islands (Fig. 13a), S_A is above 34.72 g kg^{-1} (Fig. 13b), and the DO is relatively low < 6 mL L^{-1} (Fig. 13d). The tilt of the isotherms is a signature of the Bransfield Front, which in turn is associated with the mid-depth Bransfield Current (Niiler et al., 1991; López et al., 1999; Sangrà et al., 2011). In the section between the King George Island and the Antarctic Peninsula the warm, salty and deoxygenated mCDW is still present at similar depths (Fig. 13e,f,h). Towards the bottom, Θ decreases to the lowest values in the region, characterizing the Bransfield Strait central basin. In this section, the surface Peninsula Front is visible, associated with the cold regime from the western Weddell Sea continental shelf. To the north, the signal of mCDW becomes weaker (Fig. 13i). In all sections, the dome-like shape of the isopycnals supports the cyclonic gyre presence in the region (Fig. 13c,g,k; Zhou et al., 2002; Sangrà et al., 2011; Collares et al., 2018). The circulation, mixing rates and turbulent processes are poorly explored in the NAP, thus there is a need for further studies on these processes to better comprehend the local water mass transformation in the different depth layers (e.g., Brearley et al., 2017) as it ultimately impacts the physico-chemical properties and biology of the region.

Our gridded product also distinguishes well the difference between the central and eastern basins of the Bransfield Strait (Fig. 14a-d). Colder, denser and more oxygenated deep waters are observed in the former basin, whereas the latter is relatively warmer, lighter and less oxygenated. This dichotomy occurs because the central basin has restricted connections with the adjacent region due to bathymetric constrains and it also receives more contribution from HSSW than the eastern basin (Gordon et al., 2000; Dotto et al., 2016). The section between the Elephant Island and the Joinville Island unveils the Peninsula Front associated with the shelf break at southern latitudes, where Weddell Sea-sourced waters enter the Bransfield Strait (Fig. 14e-h). At deeper layers, less oxygenated waters are observed centred at 62°S and ~500 m. This could be associated with modified Warm Deep Water entering the region, since slightly warm and salty signals are also observed at similar depth ranges (Gordon et al., 2000). However, we need to increase our comprehension on the contribution to the water mass mixture

https://doi.org/10.5194/essd-2020-244
Preprint. Discussion started: 23 September 2020

and the access routes of Warm Deep Water into the Bransfield Strait via Powell Basin to resolve the local circulation in more details (e.g., Thompson et al., 2009; Azaneu et al., 2017). Moreover, given the spatial scales and the smoothing following the gridding procedure, Bransfield Strait mesoscale and submesoscale eddies are not observed in our gridded product.

4.3 Comparison against other climatological products

Most climatological products are built to represent the global ocean and its large-scale basins, such as the Southern Ocean. The NAP, on the other hand, is a relatively small region but highly dynamical and ecologically important to connect regional environments (Kerr et al., 2018a). In this context, we now compare the GOAL gridded product with some other available gridded products, widely used by the ocean community, to show how effective is to have regional climatologies, especially in areas of intense spatial and temporal variability. For these comparisons, we chose to use the WOA and CARS climatologies and the SOSE state estimate previously described in Sect. 2. Although SOSE is based on a model, and one could argue that comparing it with a gridded product is not a fair comparison, we decided to used it because the data coverage of the Southern Ocean is relatively poor in space and time, and many studies have used SOSE as a benchmark to evaluate other ocean model outputs (e.g., Spence et al., 2017; Russell et al., 2018). In addition, SOSE has been used as initial conditions for simulations within the Bransfield Strait (e.g., Zhou et al., 2020). Despite the limitations of state estimate and ocean reanalysis (e.g., Mazloff et al., 2010; Azaneu et al., 2014; Dotto et al., 2014; Aguiar et al., 2017; Verdy and Mazloff, 2017), combining model and observations, such as in SOSE, leads to great improvements on the comprehension of the Southern Ocean dynamics (e.g., van Sebille et al., 2013; Abernathey et al., 2016; Rodriguez et al., 2016; Tamsitt et al., 2018).

The vertical water mass structure of the NAP is well represented by the GOAL gridded product (Fig. 15a,b). The density distribution and thermohaline ranges agree well with the input data, as previously shown (Sect. 4.1 and 4.2). The 2005-2017 summer-averaged WOA is colder at the surface, but the intermediate to deep ocean seems to have thermohaline range and density structure similar to observations (Fig. 15c,d). The summer-estimated CARS seems to represent well the NAP region, despite being a product with coarser resolution. It has the range of Θ and S_A in agreement with the observations throughout the water column (Fig. 15e). A good agreement is also observed for the dense waters, where CARS has similar levels of γ^n compared to the measured data (Fig. 15f). Contrary to WOA, the GOAL gridded product and the CARS climatology do not show supercooled waters centred at γ^n ~28.27 kg m^{-3}, in agreement with the observations (Fig. 15b, d and f). The 2008-2018 Februaries-averaged SOSE represents the upper ocean considerably fresher, whereas the water masses at intermediate densities levels are colder than the observations (Fig. 15g). The dense water masses ($\gamma^n > 28.27$ kg m^{-3}) are not well represented in SOSE, being considerably warmer and saltier than the observations (Fig. 15h). However, due to higher temperatures, lighter waters flood the bottom layers of SOSE. The similarity of the GOAL gridded product and the WOA and CARS climatologies to the observations is because these data sets are totally fed by in situ data, whereas SOSE is based on a model run fed by in situ data.

Now, to present the water mass structure, we show the representation of these products along the section cutting across the central and eastern basins of the Bransfield Strait. WOA unveils the upper ocean considerably colder, and despite having similar ranges of Θ as the GOAL gridded product in the mid to deep ocean, the distinction between the Bransfield Strait's central and eastern basins is not well represented (Fig. 16a). The S_A distribution in WOA is slightly saltier than the GOAL gridded product, and it does not show a clear spatial variability (Fig. 16b). For CARS, Θ climatology is in better agreement with the GOAL gridded product, both in the upper ocean and deeper layers (Fig. 16c). Although the deep Θ in CARS are not as low as the GOAL gridded product, a clear thermal distinction is observed between the central and eastern basin of the Bransfield Strait. On the other hand, the S_A field is slightly saltier in CARS than the GOAL gridded product, and the spatial distribution is less variable, as observed by the flatness of the isohalines (Fig. 16d). Interesting, however, is the representation of DO in CARS, which resembles the GOAL gridded product in terms of magnitude and spatial distribution (Fig. 16e). In both products, the DO is higher in the central basin (although slightly overestimated in CARS climatology). SOSE is considerably warmer in most of the water column in both basins (Fig. 16f) when compared to the GOAL gridded product (Fig. 14a). As discussed previously, SOSE shows higher salinity than the GOAL in both basins below ~250 m depth (Fig. 16g). Regarding DO, SOSE is oversaturated in the upper layer and highly deoxygenated bellow ~100 m (Fig. 16h), compared to GOAL (Fig. 14d). Contrary to the GOAL gridded product, the Peninsula and the Bransfield fronts are not well captured by WOA, CARS and SOSE, likely due to their coarser resolution (Fig. A1). Also, the dome-like structure of the isopycnals in the Bransfield Strait due to the cyclonic circulation is not apparent in these other products analysed (Fig. A2).

One must keep in mind that WOA and CARS are global climatologies, and their relatively low-resolution (i.e. 1/4° and 1/2°, respectively) does not represent properly some local and regional environments of the Southern Ocean, like the NAP (for instance, the distance between the South Shetland Islands and the Antarctic Peninsula is slightly higher than 100 km). Despite having lower resolution, CARS seemed to represent better the hydrographic properties in the Bransfield Strait than WOA. Although beyond the scope of this work, this discrepancy could be associated with the interpolation methods that are distinct for each climatology. On the other hand, SOSE is a state estimate where a model is constrained by observations. Although its output products are good to study and represent large scale processes, SOSE did not seem fit to be used in regional seas, at least in the NAP, where complex dynamics and contrasting regimes set the local water mass structure and variability. In this sense, simulations of regional models could be significantly impacted by the use of those large scale climatologies and reanalysis products.

In summary, the GOAL gridded product is robust enough to represent many described dynamic features of the region and, to our knowledge, its hydrographic fields closely follow the observations better than any other available products. Hence, the GOAL gridded product can be used to represent the summer mean state conditions as well as to feed ocean regional models of the highly transitional and dynamic NAP environments. However, a few caveats can be identified in the GOAL gridded product. First, it reflects only the summertime conditions of the region, as the input data was measured between January and March. Second, the grid scale (~10 km) is similar or even smaller than the first baroclinic Rossby radius of the region (Chelton

https://doi.org/10.5194/essd-2020-244
Preprint. Discussion started: 23 September 2020

et al., 1998), thus missing information of small-scale features. Third, the smoothing radius chosen in the objective interpolation and the mean state associated with the interpolation filters out most of the small dynamic features and the eddies associated with the Peninsula Front (e.g., Sangrà et al., 2011). Finally, this data set brings a novel tool and opens a plenty of possible future applications to better understand the regional circulation and hydrography along the NAP, a recognized marine climate hotspot (Kerr et al., 2018a).

5 Data availability

The time-composite GOAL gridded product is available at https://www.goal.furg.br/producao-cientifica/supplements/203-goal-gridded-nap and at https://doi.org/10.5281/zenodo.3989548 (Dotto et al., 2020), as a netCDF file. The file contains the 3D gridded variables in situ temperature (˚C), potential temperature (˚C), conservative temperature (˚C), practical salinity, absolute salinity (g kg^{-1}), neutral density (kg m^{-3}), dissolved oxygen (mL L^{-1}), and their respective relative error matrices. Depth levels (in metres) and the 2D gridded coordinates latitude and longitude are also included in the file. Missing values corresponding to relative errors > 0.5 and land mask are marked as *not a number* (NaN).

6 Conclusions

Here, we presented a novel gridded hydrographic product for the NAP region generated by optimal interpolation using the hydrographic data collected by the GOAL group between 2003-2019. The gridded product has a spatial resolution of ~10 km and 114 standard depths with spacing ranging from 5 m in the upper ocean to 75 m in depths >2200 m. The GOAL gridded product represents quite well many oceanic features of the region, such as (i) the inflows of Weddell Sea-sourced waters and the warm regime from the Bellingshausen Sea, (ii) the Peninsula and the Bransfield Fronts, (iii) the Bransfield Current signature, (iv) the cyclonic circulation within the Bransfield Strait and (v) the Bransfield Strait central and eastern basins dichotomic hydrographic regime. The latter is not well observed in some of the other products evaluated and depicting the mechanisms behind those differences still poses a challenge to the community. Due to the larger mapping errors, one must have caution when considering areas near the edge of the NAP region and as well as areas of limited data coverage. As caveats, the GOAL gridded product is a summertime composite and, therefore, does not reflect the seasonal variability of ocean properties in the NAP. In addition, the most represented regions are the Bransfield and Gerlache straits because most of the GOAL cruises sampling focused on these regions. Moreover, smaller scale features, such as eddies associated with the Peninsula Front are also not represented. Nevertheless, the GOAL gridded product is a valuable tool for setting up regional ocean models and ocean reanalysis assessment, or to any user who wants to use it to characterize the mean-summer-state hydrography of the NAP in the early 21st-century.

Author contribution. All authors designed and conceptualized the study. TSD led the study, data processing, and writing of the manuscript. RK, MMM, and CAEG lead the projects and cruises, and contributed substantially to writing the manuscript.

https://doi.org/10.5194/essd-2020-244
Preprint. Discussion started: 23 September 2020

Competing interests. The authors declare that they have no conflict of interest.

Acknowledgement. This study is part of the activities of the Brazilian High Latitude Oceanography Group (GOAL) within the Brazilian Antarctic Program (PROANTAR). GOAL has been funded by and/or has received logistical support from the Brazilian Ministry of the Environment (MMA), the Brazilian Ministry of Science, Technology, and Innovation (MCTI), the Council for Research and Scientific Development of Brazil (CNPq), the Brazilian Navy, the Inter-Ministerial Secretariat for Sea Resources (SECIRM), the National Institute of Science and Technology of the Cryosphere (INCT CRIOSFERA; CNPq grants No. 573720/2008-8 and 465680/2014-3) and the Research Support Foundation of the State of Rio Grande do Sul (FAPERGS grant No. 17/2551-000518-0). This study was conducted within the activities of the REDE-1, SOS-CLIMATE, POLARCANION, PRO-OASIS, NAUTILUS, INTERBIOTA, PROVOCCAR and ECOPELAGOS projects (CNPq grants No. 550370/2002-1, 520189/2006-0, 556848/2009-8, 565040/2010-3, 405869/2013-4, 407889/2013-2, 442628/2018-8 and 442637/2018-7, respectively). Financial support was also received from Coordination for the Improvement of Higher Education Personnel (CAPES) through the project CAPES "Ciências do Mar" (grant No. 23038.001421/2014-30). CAPES also provided free access to many relevant journals though the portal "Periódicos CAPES", and the activities of the Graduate Program in Oceanology. T.S. Dotto acknowledge financial support from CNPq PDJ scholarship grant No. 151248/2019-2. R. Kerr, M. M. Mata and C. A. E. Garcia are granted with researcher fellowships from CNPq grants No. 304937/2018-5, 306896/2015-0, 309932/2019-0, respectively. The authors thank to the officers and crew of the polar vessels *Ary Rongel* and *Almirante Maximiano* of the Brazilian Navy, and the several scientists and technicians participating in the cruises for their valuable help during data sampling and data processing.

References

Abernathey, R., Cerovecki, I., Holland, P. et al. Water-mass transformation by sea ice in the upper branch of the Southern Ocean overturning, Nature Geoscience, 9, 596–601, doi: 10.1038/ngeo2749, 2016.

Aguiar, W., Mata, M. M., and Kerr, R.: On deep convection events and Antarctic Bottom Water formation in ocean reanalysis products, Ocean Science, 13, 851–872, doi: 10.5194/os-13-851-2017, 2017.

Azaneu, M., Kerr, R., Mata, M. M., and Garcia, C. A. E.: Trends in the deep Southern Ocean (1958–2010): Implications for Antarctic Bottom Water properties and volume export, Journal of Geophysical Research: Oceans, 118, 4213–4227, doi: 10.1002/jgrc.20303, 2013.

Azaneu, M., Kerr, R., and Mata, M. M.: Assessment of the representation of Antarctic bottom water properties in the ECCO2 reanalysis, Ocean Sci., 10, 923–946, doi:10.5194/os-10-923-2014, 2014.

Azaneu, M., Heywood, K. J., Queste, B. Y., and Thompson, A. F.: Variability of the Antarctic Slope Current System in the Northwestern Weddell Sea, Journal of Physical Oceanography, 47, 2977–2997, doi: 10.1175/JPO-D-17-0030.1, 2017.

https://doi.org/10.5194/essd-2020-244
Preprint. Discussion started: 23 September 2020

Brearley, J. A., Meredith, M. P., Naveira Garabato, A. C., Venables, H. J. and Inall, M. E.: Controls on turbulent mixing on the West Antarctic Peninsula shelf, Deep Sea Research Part II, 139, 18-30, doi: 10.1016/j.dsr2.2017.02.011, 2017.

Bretherton, F. P., Davis, R. E., and Fandry, C. B.: A technique for objective analysis and design of oceanographic experiments applied to mode-73, Deep-Sea Research and Oceanographic Abstracts, 23, 559–582, doi:10.1016/0011-7471(76)90001-2, 1976.

Carpenter, J.H.: The Chesapeake Bay institute technique for the Winkler dissolved oxygen titration, Limnology and Oceanography, 10, 141–143, doi: 10.4319/lo.1965.10.1.0141, 1965.

Chelton, D. B., deSzoeke, R. A., Schlax, M. G., El Naggar, K. and Siwertz, N.: Geographical Variability of the First Baroclinic Rossby Radius of Deformation, Journal of Physical Oceanography, 28, 433–460, doi: 10.1175/1520-0485(1998)028<0433:GVOTFB>2.0.CO;2, 1998.

Collares, L., Mata, M. M., Kerr, R., Arigony Neto, J. and Barbat, M. M.: Iceberg drift and ocean circulation in the Northwestern Weddell Sea, Antarctica, Deep Sea Research Part II, 149, 10-24, doi: 10.1016/j.dsr2.2018.02.014, 2018.

Cook, A. J., Holland, P. R., Meredith, M. P., Murray, T., Luckman, A. and Vaughan, D. G.: Ocean forcing of glacier retreat in the western Antarctic Peninsula. Science, 353 (6296), 283–286, doi: 10.1126/science.aae0017, 2016 .

Costa, R. R., Mendes, C. R. B., Tavano, V. M., Dotto, T. S., Kerr, R., Monteiro, T., Odebrecht, C. and Secchi, E. R.: Dynamics of an intense diatom bloom in the Northern Antarctic Peninsula, February 2016, Limnology and Oceanography, doi: 10.1002/lno.11437, 2020.

Couto, N., Martinson, D. G., Kohut, J. and Schofield, O.: Distribution of Upper Circumpolar Deep Water on the warming continental shelf of the West Antarctic Peninsula, Journal of Geophysical Research: Oceans, 122, 5306–5315, doi: 10.1002/2017JC012840, 2017.

Culberson, C. H., Knapp, G. P., Stalcup, M. C., Williams, R. T., and Zemlyak, F.: A comparison of methods for the determination of dissolved oxygen in seawater, Report WHPO 91-2, WOCE Hydrographic Programme Office, 1991-08, doi:10.1575/1912/243, 1991.

Detoni, A. M., de Souza, M. S., Garcia, C. A., Tavano, V. M. and Mata, M. M.: Environmental conditions during phytoplankton blooms in the vicinity of James Ross Island, east of the Antarctic Peninsula. Polar Biology, 38 (8), 1111–1127, 2015.

Dinniman, M. S., Klinck, J. M., and Hofmann, E. E.: Sensitivity of Circumpolar Deep Water Transport and Ice Shelf Basal Melt along the West Antarctic Peninsula to Changes in the Winds, Journal of Climate, 25, 4799–4816, doi: 10.1175/JCLI-D-11-00307.1, 2012.

Dotto, T. S., Kerr, R., Mata, M. M., Azaneu, M., Wainer, I., Fahrbach, E. and Rohardt, G.: Assessment of the structure and variability of Weddell Sea water masses in distinct ocean reanalysis products, Ocean Sci., 10, 523–546, doi:10.5194/os-10-523-2014, 2014.

Dotto, T. S., Kerr, R. Mata, M. M., and Garcia, C. A. E.: Multidecadal freshening and lightening in the deep waters of the Bransfield Strait, Antarctica, J. Geophys. Res. Oceans, 121, 3741–3756, doi:10.1002/2015JC011228, 2016.

https://doi.org/10.5194/essd-2020-244
Preprint. Discussion started: 23 September 2020

Dotto, T. S., Kerr, R., Mata, M. M., and Garcia, C. A. E. (2020). GOAL hydrographic gridded data set for the Northern Antarctic Peninsula, Southern Ocean [Data set], Zenodo, doi:10.5281/zenodo.3989548, 2020.

García, M.A., Castro, C. G., Ríos, A. F., Doval, M. D., Rosón, G., Gomis, D. and López, O.: Water masses and distribution of physico-chemical properties in the Western Bransfield Strait and Gerlache Strait during Austral summer 1995/96, Deep-Sea Research Part II, 49, 585–602, doi: 10.1016/S0967-0645(01)00113-8, 2002.

Gonçalves-Araujo, R., de Souza, M. S., Tavano, V. M. and Garcia, C. A. E.: Influence of oceanographic features on spatial and interannual variability of phytoplankton in the Bransfield Strait, Antarctica, Journal or Marine System, 142, 1–15, doi: 10.1016/j.jmarsys.2014.09.007, 2015.

Gordon, A. L., Mensch, M., Zhaoqian, D., Smethie, W. M. and de Bettencourt, J.: Deep and bottom water of the Bransfield Strait eastern and central basins, Journal of Geophysical Research, 105(C5), 11,337–11,346, doi: 10.1029/2000JC900030, 2000.

Hellmer, H. H., Huhn, O., Gomis, D. and Timmermann, R.: On the freshening of the northwestern Weddell Sea continental shelf, Ocean Science, 7, 305–316, doi: 10.5194/os-7-305-2011, 2011.

Heywood, K. J., Naveira Garabato, A. C., Stevens, D. P. and Muench, R. D.: On the fate of the Antarctic Slope Front and the origin of the Weddell Front, Journal of Geophysical Research, 109, C06021, doi: 10.1029/2003JC002053, 2004.

Hogg, A. McC., Meredith, M. P., Chambers, D. P., Abrahamsen, E. P., Hughes, C. W. and Morrison, A. K.: Recent trends in the Southern Ocean eddy field, J. Geophys. Res. Oceans, 120, 257–267, doi:10.1002/2014JC010470, 2015.

Huneke, W. G. C., Huhn, O. and Schröeder, M.: Water masses in the Bransfield Strait and adjacent seas, austral summer 2013, Polar Biology, 39, 789–798, doi: 10.1007/s00300-016-1936-8, 2016.

Jackett, D., and McDougall, T.: A neutral density variable for the world's ocean, Journal of Physical Oceanography, 27, doi: 10.1175/1520-0485(1997)027<0237:ANDVFT>2.0.CO;2, 1997.

Kerr, R., Mata, M. M., Mendes, C. R. B. and Sechhi, E. R.: Northern Antarctic Peninsula: a marine climate hotspot of rapid changes on ecosystems and ocean dynamics, Deep Sea Research Part II, 149, 4–9, doi: 10.1016/j.dsr2.2018.05.006, 2018a.

Kerr, R., Goyet, C., da Cunha L. C., Orselli, I. O., Lencina-Avila, J. M., Mendes, C. R. B., Mata, M. M. and Tavano, V. M.: Carbonate system properties in the Gerlache Strait, Northern Antarctic Peninsula (February 2015): II. Anthropogenic CO2 and seawater acidification, Deep Sea Research Part II, 149, 182-192, doi: 10.1016/j.dsr2.2017.07.007, 2018b.

Lencina-Avila, J. M., Goyet, C., Kerr, R., Orselli, I. B. M., Mata, M. M., and Touratier, F.: Past and future evolution of the marine carbonate system in a coastal zone of the Northern Antarctic Peninsula, Deep Sea Research Part II, 149, 193-205, doi: 10.1016/j.dsr2.2017.10.018, 2018.

Lin, X., Zhai, X., Wang, Z., and Munday, D. R.: Mean, Variability, and Trend of Southern Ocean Wind Stress: Role of Wind Fluctuations, Journal of Climate, 31, 3557–3573, doi:10.1175/JCLI-D-17-0481.1, 2018.

Locarnini, R. A., Mishonov, A. V., Baranova, O. K., Boyer, T. P., Zweng, M. M., Garcia, H. E., Reagan, J. R., Seidov, D., Weathers, K., Paver, C. R. and Smolyar, I.: World Ocean Atlas 2018, Volume 1: Temperature. A. Mishonov Technical Ed.; NOAA Atlas NESDIS 81, 52 pp., 2018.

https://doi.org/10.5194/essd-2020-244
Preprint. Discussion started: 23 September 2020

Loeb, V. J., Hofmann, E. E., Klinck, J. M., Holm-Hansen, O. and White, W. B.: ENSO and variability of the Antarctic Peninsula pelagic marine ecosystem, Antarctic Science, 21 (2), 135–148, doi: 10.1017/S0954102008001636, 2009.

López, O., García, M. A., Gomis, D., Rojas, P., Sospedra, J., S.-Arcilla, A.: Hydrographic and hydrodynamic characteristics ofthe eastern basin of the Bransfield Strait (Antarctica), Deep-Sea Research Part I, 46, 1755–1778, doi: 10.1016/S0967-0637(99)00017-5, 1999.

Marshall, G.: Trends in the Southern annular mode from observations and reanalyses, Journal of Climate, 16, 4134–4143, doi: 10.1175/1520-0442(2003)016<4134:TITSAM>2.0.CO;2, 2003.

Mata, M. M., Tavano, V. M. and Garcia, C. A. E.: 15 years sailing with the Brazilian High Latitude Oceanography Group (GOAL), Deep Sea Research Part II, 149, 1-3, doi: 10.1016/j.dsr2.2018.05.007, 2018.

Mata, M. M. and Garcia, C. A. E.: Physical oceanography during Ary Rongel cruise GOAL2003. PANGAEA, https://doi.org/10.1594/PANGAEA.863598, 2016a.

Mata, M. M. and Garcia, C. A. E.: Physical oceanography during Ary Rongel cruise GOAL2004. PANGAEA, https://doi.org/10.1594/PANGAEA.863599, 2016b.

Mata, M. M. and Garcia, C. A. E.: Physical oceanography during Ary Rongel cruise GOAL2005. PANGAEA, https://doi.org/10.1594/PANGAEA.863600, 2016c.

Mata, M. M. and Garcia, C. A. E.: Physical oceanography during Ary Rongel cruise SOS-Climate I. PANGAEA, https://doi.org/10.1594/PANGAEA.864576, 2016d.

Mata, M. M. and Garcia, C. A. E.: Physical oceanography during Ary Rongel cruise SOS-Climate II. PANGAEA, https://doi.org/10.1594/PANGAEA.864578, 2016e.

Mata, M. M. and Garcia, C. A. E.: Physical oceanography during Ary Rongel cruise SOS-Climate III. PANGAEA, https://doi.org/10.1594/PANGAEA.864579, 2016f.

Mata, M. M. and Kerr, R.: Physical oceanography during Ary Rongel cruise POLARCANION-I. PANGAEA, https://doi.org/10.1594/PANGAEA.864591, 2016a.

Mata, M. M. and Kerr, R.: Physical oceanography during Almirante Maximiano cruise POLARCANION-II. PANGAEA, https://doi.org/10.1594/PANGAEA.864592, 2016b.

Mata, M. M. and Kerr, R.: Physical oceanography during Almirante Maximiano cruise POLARCANION-III. PANGAEA, https://doi.org/10.1594/PANGAEA.864593, 2016c.

Mazloff, M. R., Heimbach, P. and Wunsch, C.: An Eddy-Permitting Southern Ocean State Estimate, Journal of Physical Oceanography, 40, 880–899, doi: 10.1175/2009JPO4236.1, 2010.

McDougall, T. J., and Barker, P. M.: Getting started with TEOS-10 and the Gibbs Seawater (GSW) Oceanographic Toolbox. SCOR/IAPSO WG127, 28pp., ISBN 978-0-646-55621-5, 2011.

McKee, D. C., and Martinson, D. G.: Spatially coherent intraseasonal velocity fluctuations on the western Antarctic Peninsula shelf, Journal of Geophysical Research: Oceans, 125, e2019JC015770, doi: 10.1029/2019JC015770, 2020.

https://doi.org/10.5194/essd-2020-244
Preprint. Discussion started: 23 September 2020

Martinson, D. G. and McKee, D. C.: Transport of warm Upper Circumpolar Deep Water onto the western Antarctic Peninsula continental shelf, Ocean Sci., 8, 433–442, https://doi.org/10.5194/os-8-433-2012, 2012.

Mendes, C. R. B., de Souza, M. S., Garcia, V. M. T., Leal, M. C., Brotas, V. and Garcia, C. A. E.: Dynamics of phytoplankton communities during late summer around the tip of the Antarctic Peninsula, Deep Sea Research Part I, 65, 1–14, doi: 10.1016/j.dsr.2012.03.002, 2012.

Mendes, C. R. B., Tavano, V. M., Leal, M. C., de Souza, M. S., Brotas, V. and Garcia, C. A. E.: Shifts in the dominance between diatoms and cryptophytes during three late summers in the Bransfield Strait (Antarctic Peninsula), Polar Biology, 36 (4), 537–547, doi: 10.1007/s00300-012-1282-4, 2013.

Meredith, M. P., and Hogg, A. M.: Circumpolar response of Southern Ocean eddy activity to a change in the Southern Annular Mode, Geophysical Research Letters, 33, L16608, doi: 10.1029/2006GL026499, 2006.

Meredith, M. P., and King, J. C.: Rapid climate change in the ocean west of the Antarctic Peninsula during the second half of the 20th century, Geophysical Research Letters, 32, L19604, doi:10.1029/2005GL024042, 2005

Meredith, M. P., Schofield, O., Newman, L., Urban, E., and Sparrow, M.: The vision for a Southern Ocean Observing System, Current Opinion in Environmental Sustainability, 5, 3–4, doi: 10.1016/j.cosust.2013.03.002, 2013.

Moline, M. A., Claustre, H., Frazer, T. K., Schofield, O. and Vernet, M.: Alteration of the food web along the Antarctic Peninsula in response to a regional warming trend, Global Change Biology, 10, 1973-1980, doi: 10.1111/j.1365-2486.2004.00825.x, 2004.

Montes-Hugo, M., Doney, S. C., Duclow, H. W., Fraser, W., Martinson, D., Stammerjohn, S. E. and Schofield, O.: Recent changes in phytoplankton communities associated with rapid regional climate change along the Western Antarctic Peninsula, Science, 323, 1470–1473. doi:10.1126/science.1164533, 2009.

Newman, L., Heil, P., Trebilco, R., Katsumata, K., Constable, A., van Wijk, E., Assmann, K., Beja, J., Bricher, P., Coleman, R., Costa, D., Diggs, S., Farneti, R., Fawcett, S., Gille, S. T., Hendry, K. R., Henley, S., Hofmann, E., Maksym, T., Mazloff, M., Meijers, A., Meredith, M. M., Moreau, S., Ozsoy, B., Robertson, R., Schloss, I., Schofield, O., Shi, J., Sikes, E., Smith, I. J., Swart, S., Wåhlin, A., Williams, G., Williams, M. J. M., Herraiz-Borreguero, L., Kern, S., Lieser, J., Massom, R. A., Melbourne-Thomas, J., Miloslavich, P. and Spreen, G.: Delivering Sustained, Coordinated, and Integrated Observations of the Southern Ocean for Global Impact, Frontiers in Marine Science, 6:433, doi: 10.3389/fmars.2019.00433, 2019.

Niiler, P. P., Amos, A., and Hu, J.-H.: Water masses and 200 m relative geostrophic circulation in the western Bransfield Strait region, Deep Sea Res., Part A, 38, 943–959, doi:10.1016/0198-0149(91)90091-S, 1991.

Renner, A. H. H., Thorpe, S. E., Heywood, K. J., Murphy, E. J., Watkins, J. L., and Meredith, M. P.: Advective pathways near the tip of the Antarctic Peninsula: Trends, variability and ecosystem implications, Deep Sea Research Part I, 63, 91–101, doi:10.1016/j.dsr.2012.01.009, 2012.

Ridgway K.R., Dunn, J. R. and Wilkin J. L.: Ocean interpolation by four-dimensional least squares -Application to the waters around Australia, Journal of Atmospheric and Oceanic Technology, 19, 1357-1375, doi: 10.1175/1520-0426(2002)019<1357:OIBFDW>2.0.CO;2, 2002.

https://doi.org/10.5194/essd-2020-244
Preprint. Discussion started: 23 September 2020

Rignot, E., Mouginot, J., Scheuchl, B., van den Broeke, M., van Wessem, M. J. and Morlighem, M.: Four decades of Antarctic Ice Sheet mass balance from 1979-2017, Proceeding of the National Academy of Sciences of the United States of America, 116(4), 1095-1103, doi: 10.1073/pnas.1812883116, 2019.

Rodriguez, A. R., Mazloff, M. R. and Gille, S. T.: An oceanic heat transport pathway to the Amundsen Sea Embayment, Journal of Geophysical Research: Oceans, 121, 3337-3349, doi: 10.1002/2015JC011402, 2016.

Ruiz-Barlett, E. M., Tosonotto, G. V., Piola, A. R., Sierra, M. A. and Mata, M. M.: On the temporal variability of intermediate and deep waters in the Western Basin of the Bransfield Strait, Deep Sea Research Part II, 149, 31-46, doi: 10.1016/j.dsr2.2017.12.010, 2018.

Russell, J. L., Kamenkovich, I., Bitz, C., Ferrari, R., Gille, S. T., Goodman, P. J., et al.: Metrics for the evaluation of the Southern Ocean in coupled climate models and earth system models, Journal of Geophysical Research: Oceans, 123, 3120–3143, doi: 10.1002/2017JC013461, 2018.

Sangrà, P., Gordo, C., Hernández-Arencibia, M., Marrero-Díaz, A., Rodríguez-Santana, A., Stegner, A., Martínez-Marrero, A., Pelegrí, J. L. and Pichon, T.: The Bransfield current system, Deep Sea Research Part I, 58, 390–402, doi: 10.1016/j.dsr.2011.01.011, 2011.

Sangrà, P., Stegner, A., Hernández-Arencibia, M., Marrero-Díaz, Á., Salinas, C., Aguiar-González, B. and Mouriño-Carballido, B.: The Bransfield gravity current, Deep Sea Research Part I, 119, 1–15, doi: 10.1016/j.dsr.2016.11.003, 2017.

Savidge, D. K. and Amft, J. A.: Circulation on the West Antarctic Peninsula derived from 6 years of shipboard ADCP transects, Deep Sea Resaerch Part I, 59, 1633-1655, doi: 10.1016/j.dsr.2009.05.011, 2009.

Smith, D. A., Hofmann, E. E., Klinck, J. M. and Lascara, C. M.: Hydrography and circulation of the West Antarctic Peninsula Continental Shelf, Deep Sea Research Part I, 46, 925-949, doi: 10.1016/S0967-0637(98)00103-4, 1999.

Spence, P. S., Holmes, R. M., Hogg, A. M., Griffies, S. M., Stewart, K. D. and England, M. H.: Localized rapid warming of West Antarctic subsurface waters by remote winds, Nature Climate Change, 7, 595–603, doi: 10.1038/nclimate3335, 2017.

Stammerjohn, S. E., Martinson, D. G., Smith, R. C. and Iannuzzi, R.A.: Sea ice in the western Antarctic Peninsula region: Spatio-temporal variability from ecological and climate change perspectives, Deep Sea Research Part II, 55 (18–19), 2041–2058, doi: 10.1016/j.dsr2.2008.04.026, 2008.

Swart, N. C., and Fyfe, J. C.: Observed and simulated changes in the Southern Hemisphere surface westerly wind-stress, Geophysical Research Letters, 39, L16711, doi:10.1029/2012GL052810, 2012.

Tamsitt, V., Drake, H. F., Morrison, A. K. et al.: Spiraling pathways of global deep waters to the surface of the Southern Ocean, Nature Communications, 8, 172, doi: 10.1038/s41467-017-00197-0, 2017.

Thompson, A. F., Heywood, K. J., Thorpe, S. E. Renner, A. H. H., and Trasviña, A.: Surface circulation at the tip of the Antarctic Peninsula from drifters, Journal of Physical Oceanography, 39, 3–26, doi:10.1175/2008JPO3995.1, 2009.

Thomson, R. E. and Emery, W. J.: The Spatial Analyses of Data Fields, in: Data Analysis Methods in Physical Oceanography (Third Edition), edited by: Thomson, R. E. and Emery, W. J., Elsevier, 313-424, doi: 10.1016/B978-0-12-387782-6.00004-1, 2014.

https://doi.org/10.5194/essd-2020-244
Preprint. Discussion started: 23 September 2020

Torres Parra, R. R., Caicedo, A. L. and Sánchez, J. D. I.: Hydrographic conditions during two austral summer situations (2015 and 2017) in the Gerlache and Bismarck straits, northern Antarctic Peninsula, Deep Sea Research Part I, 161, 103278, doi: 10.1016/j.dsr.2020.103278, 2020.

Turner, J., Hosking, J. S., Phillips, T. and Marshall, G. J.: Temporal and spatial evolution of the Antarctic sea ice prior to the September 2012 record maximum extent, Geophysical Research Letters, 40, 5894–5898, doi: 10.1002/2013GL058371, 2013.

van Caspel, M., Schroeder, M., Huhn, O., and Hellmer, H. H.: Precursors of Antarctic bottom water formed on the continental shelf off Larsen ice shelf, Deep Sea Research Part I, 99, 1–9, doi: 10.1016/j.dsr.2015.01.004, 2015.

van Caspel, M. R., Mata, M. M. and Hellmer, H. H.: On the ventilation of Bransfield Strait deep basins, Deep Sea Research Part II, 149, 25-30, doi: 10.1016/j.dsr2.2017.09.006, 2018. van Sebille, E., Spence, P., Mazloff, M. R., England, M. H., Rintoul, S. R. and Saenko, O. A.: Abyssal connections of Antarctic Bottom Water in a Southern Ocean State Estimate, Geophysical Research Letters, 40, 2177–2182, doi: 10.1002/grl.50483, 2013.

von Gyldenfeldt, A. B., Fahrbach, E., García, M. A., and Schröder, M.: Flow variability at the tip of the Antarctic Peninsula, Deep Sea Research Part II, 49(21), 4743-4766, doi: 10.1016/S0967-0645(02)00157-1, 2002.

Verdy, A. and Mazloff, M. R.: A data assimilating model for estimating Southern Ocean biogeochemistry, Journal of Geophysical Research: Oceans, 122, 6968–6988, doi:10.1002/2016JC012650, 2017.

Zhou, M., Niiler, P. P. and Hu, J.-H.: Surface currents in the Bransfield and Gerlache Straits, Antarctica, Deep Sea Res., Part I, 49(2), 267–280, doi: 10.1016/S0967-0637(01)00062-0, 2002.

Zhou, M., Niiler, P. P., Zhu, Y. and Dorly, R. D.: The western boundary current in the Bransfield Strait, Antarctica, Deep-Sea Research Part I, 53, 1244–1252, doi: 10.1016/j.dsr.2006.04.003, 2006.

Zhou, X., Zhu, G. and Hu, S.: Influence of tides on mass transport in the Bransfield Strait and the adjacent areas, Antarctic, Polar Science, 23, 100506, doi: 10.1016/j.polar.2020.100506, 2020.

Zweng, M. M., Reagan, J. R., Seidov, D., Boyer, T. P., Locarnini, R. A., Garcia, H. E., Mishonov, A. V., Baranova, O. K., Weathers, K., Paver, C. R. and Smolyar, I.: World Ocean Atlas 2018, Volume 2: Salinity. A. Mishonov Technical Ed.; NOAA Atlas NESDIS 82, 50 pp., 2018

https://doi.org/10.5194/essd-2020-244
Preprint. Discussion started: 23 September 2020

Open Access Earth System Science Data Discussions

Table 1. Brazilian High Latitude Group (GOAL) projects, period of cruise, main areas sampled and variables used to generate the GOAL gridded product. Temperature (T), Conductivity (C) and dissolved oxygen (DO). Relevant references that previously used the original dataset are indicated.

GOAL project	Period of cruise	Study region in the NAP	Property	References
REDE-1	23-Jan to 23-Feb 2003	Bransfield Strait, Gerlache Strait	T, C	Gonçalves-Araújo et al., 2015
	18-Jan to 29-Jan 2004	Bransfield Strait, Gerlache Strait	T, C, DO	
	28-Jan to 07-Feb 2005	Bransfield Strait, northwestern Weddell Sea	T, C	
SOS-CLIMATE	21-Feb to 04-Mar 2008	Bransfield Strait, southern Drake Passage, northwestern Weddell Sea	T, C, DO	Mendes et al., 2012; Detoni et al., 2015
	17-Feb to 01-Mar 2009	Bransfield Strait, northwestern Weddell Sea	T, C, DO	
	16-Feb to 24-Feb 2010	Bransfield Strait, northwestern Weddell Sea	T, C, DO	
POLARCANION/PRO-OASIS	27-Feb to 04-Mar 2011	Bransfield Strait, northwestern Weddell Sea	T, C, DO	Azaneu et al., 2013; Dotto et al., 2016
	12-Feb to 03-Mar 2013	Bransfield Strait, Gerlache Strait, southern Drake Passage	T, C, DO	
	08-Feb to 24-Feb 2014	Bransfield Strait, Gerlache Strait, southern Drake Passage	T, C, DO	
NAUTILUS/INTERBIOTA	08-Feb to 17-Feb 2015	Bransfield Strait, Gerlache Strait	T, C, DO	Kerr et al., 2018a, b; Lencina-Avila et al., 2018; Costa et al., 2020; Monteiro et al., 2020
	13-Feb to 25-Feb 2016	Bransfield Strait, Gerlache Strait, Bellingshausen Sea	T, C, DO	
	14-Feb to 04-Mar 2017	Bransfield Strait, Gerlache Strait, Bellingshausen Sea	T, C, DO	
	14-Feb to 26-Feb 2018	Bransfield Strait, Gerlache Strait, Bellingshausen Sea	T, C	
	08-Jan to 31-Jan 2019	Bransfield Strait, Gerlache Strait, Bellingshausen Sea, southern Drake Passage, northwestern Weddell Sea	T, C, DO	

https://doi.org/10.5194/essd-2020-244
Preprint. Discussion started: 23 September 2020

Table 2. Standard depth levels (m) used to linearly interpolate the profiles and the gridded data set.

Level number	Depth interval	Depth range
1 to 10	5 m	5-50 m
11 to 25	10 m	55-200 m
26 to 40	20 m	220-500 m
41 to 60	25 m	525-1000 m
61 to 84	50 m	1050-2200 m
85 to 114	75 m	2275-4450 m

https://doi.org/10.5194/essd-2020-244
Preprint. Discussion started: 23 September 2020

Open Access Earth System Science Data Discussions

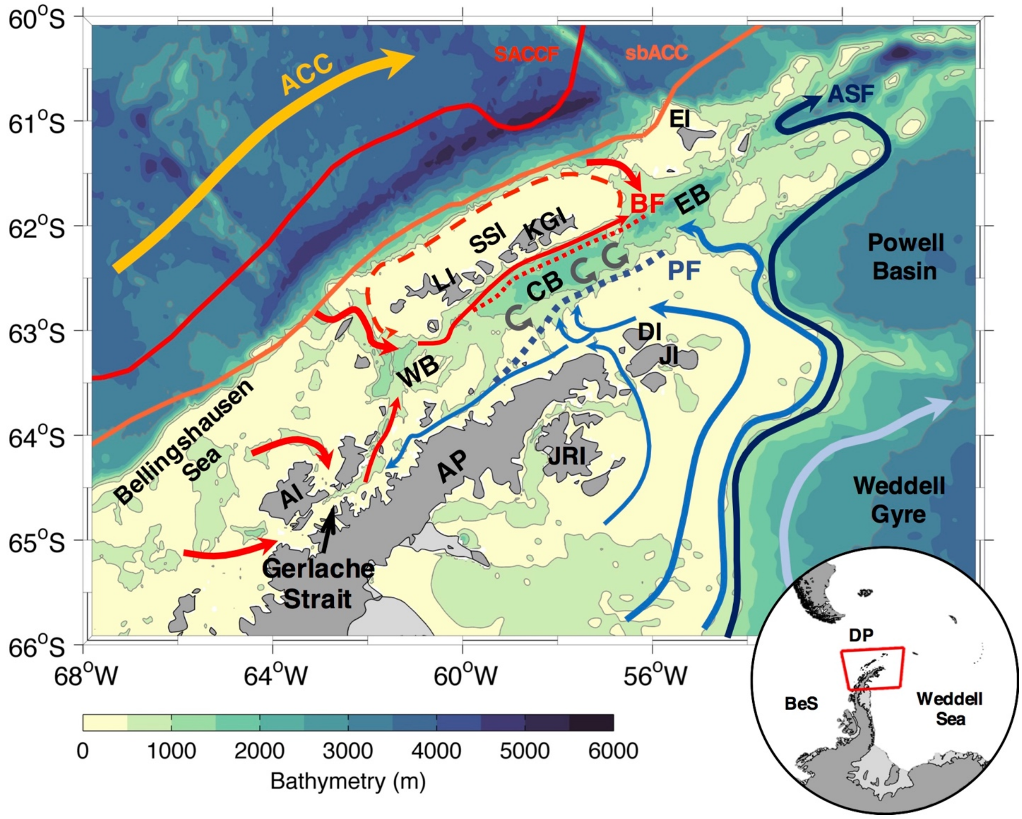

Figure 1. Schematic of the mean circulation at the Northern Antarctic Peninsula (NAP). Blue (red) arrows shows the cold (warm) water masses that inflow in the region. Cyan arrow shows the Weddell Gyre circulation and the dark blue arrow the path of the Antarctic Slope Front (ASF). Dotted blue and red lines depict, respectively, the Peninsula Front (PF) and the Bransfield Front (BF). Dashed line shows the recirculation around the South Shetland Islands (SSI). Antarctic Peninsula (AP), Elephant Island (EI), Joinville Island (JI), D'Urville Island (DI), James Ross Island (JRI), King George Island (KGI), Livingston Island (LI), and Anvers Island (AI) are shown. Within the Bransfield Strait, the area is divided in eastern basin (EB), central basin (CB) and western basin (WB). The Antarctic Circumpolar Current (ACC), the Southern ACC Front (SACCF) and the Southern Boundary of the ACC (sbACC), are shown in orange tones. Bathymetry from ETOPO1. Inset shows the study region, among the Weddell Sea, Bellingshausen Sea (BeS) and the Drake Passage (DP). Coastline from SCAR Antarctic Digital Database.

https://doi.org/10.5194/essd-2020-244
Preprint. Discussion started: 23 September 2020

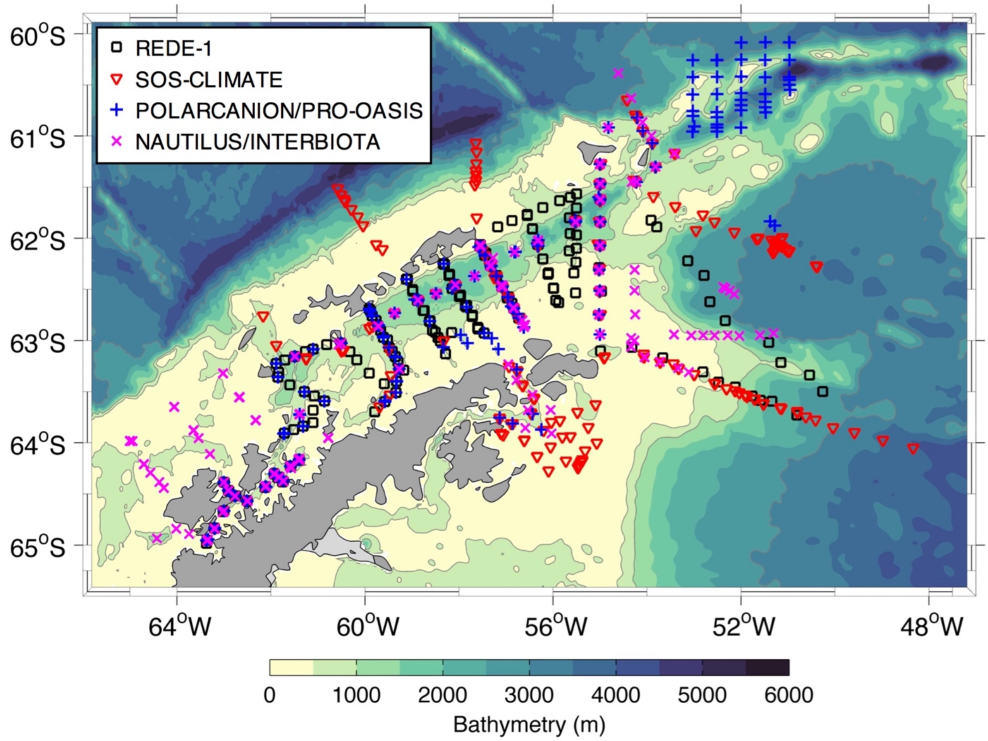

640

Figure 2. Hydrographic stations occupied by the Brazilian High Latitude Oceanography Group (GOAL) between 2003-2019. Six projects were conducted by the group, collecting a total of 895 hydrographic stations. REDE-1 (squares) run from 2003-2005, SOS-CLIMATE (triangles) between 2008-2010, POLARCANION/PRO-OASIS (plus) between 2011-2014, and NAUTILUS/INTERBIOTA (cross) between 2015-2019. See Table 1 for more information. Bathymetry from ETOPO1. Coastline from SCAR Antarctic Digital Database.

645

https://doi.org/10.5194/essd-2020-244
Preprint. Discussion started: 23 September 2020

Open Access Earth System Science Data Discussions

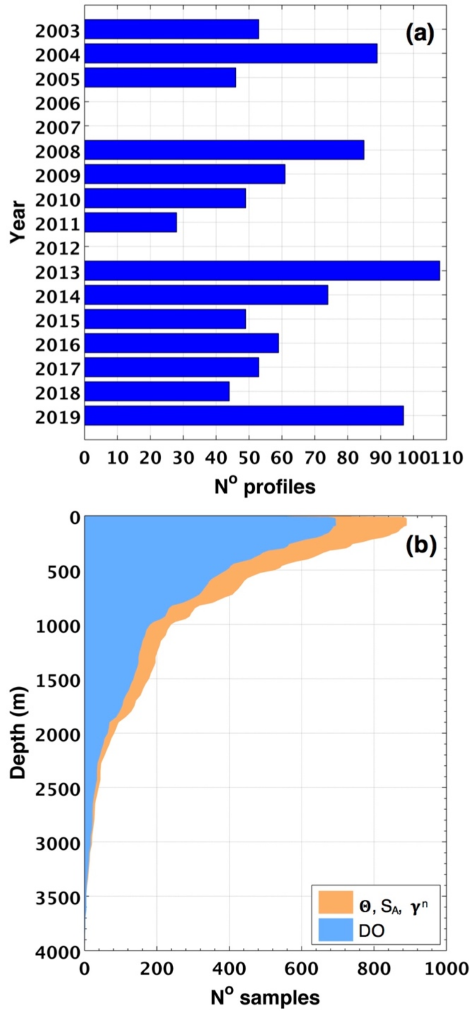

Figure 3. (a) Number of hydrographic stations per year and, (b) number of samples binned into the standard depth levels for conservative temperature (Θ), absolute salinity (SA), neutral density (γ^n), in orange, and dissolved oxygen (DO), in blue.

https://doi.org/10.5194/essd-2020-244
Preprint. Discussion started: 23 September 2020

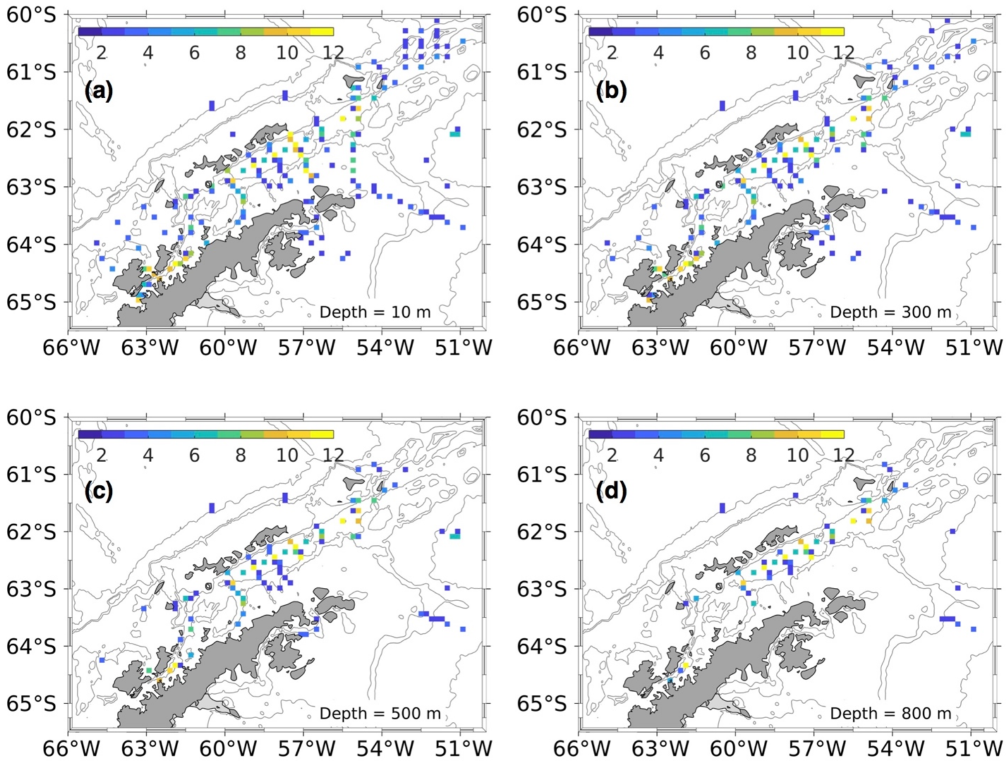

650

Figure 4. Number of hydrographic stations occupied within each grid cell of the domain in different depths between 2003-2019. (a) 10 m, (b) 300 m, (c) 500 m, and (d) 800 m. ETOPO1 isobaths of 500 m, 1000 m and 3000 m are depicted by black lines. Coastline from SCAR Antarctic Digital Database.

655

https://doi.org/10.5194/essd-2020-244
Preprint. Discussion started: 23 September 2020

Open Access Earth System Science Data Discussions

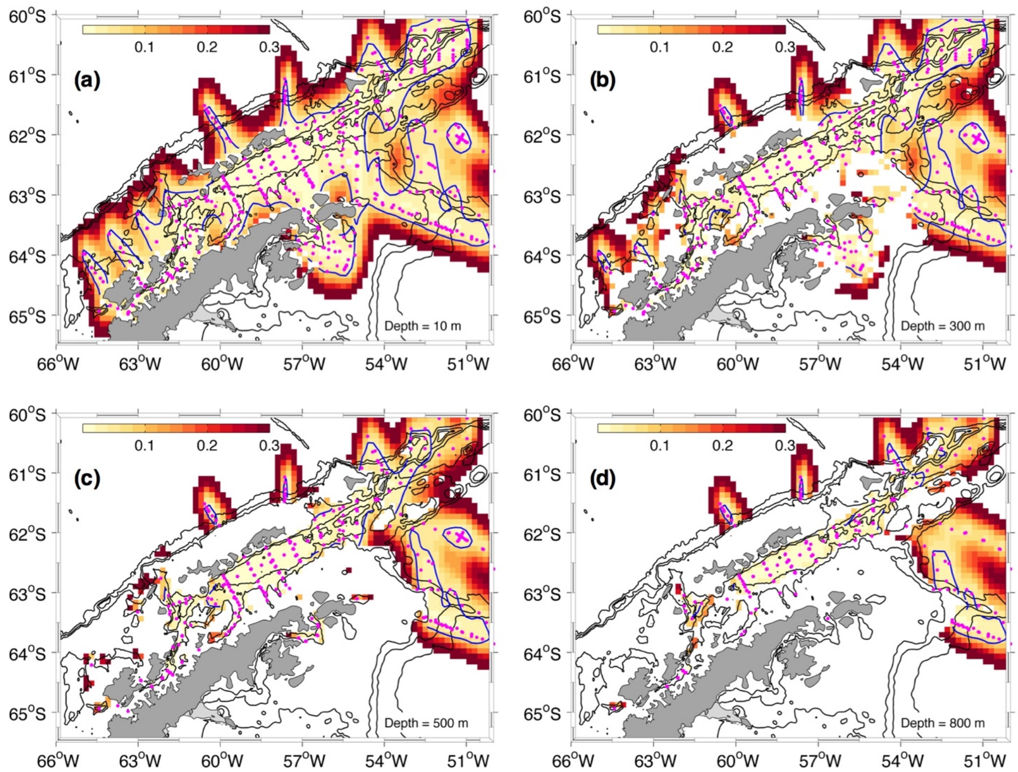

660 **Figure 5.** Conservative temperature relative error calculated in the objective interpolation for different depths. (a) 10 m, (b) 300 m, (c) 500 m, and (d) 800 m. Magenta dots depict the hydrographic stations for each depth. Relative error of 0.05 is marked by the blue line. Areas where the relative error is > 0.5 are blank. ETOPO1 isobaths of 500 m, 1000 m and 3000 m are depicted by black lines. Coastline from SCAR Antarctic Digital Database.

https://doi.org/10.5194/essd-2020-244
Preprint. Discussion started: 23 September 2020

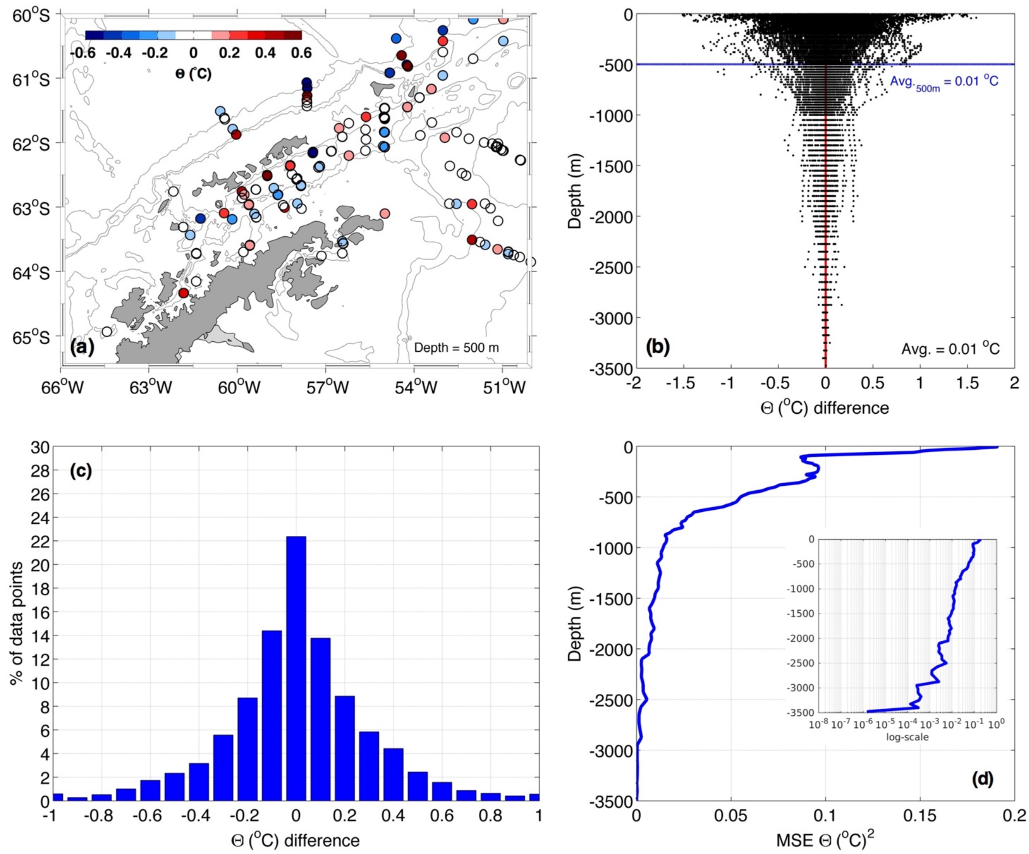

Figure 6. Difference between the gridded product and the hydrographic stations closer ~6 km at 500 m depth for (a) conservative temperature (Θ; °C). ETOPO1 isobaths of 500 m, 1000 m and 3000 m are depicted by black lines in (a). Coastline from SCAR Antarctic Digital Database. (b) Θ vertical difference between the gridded product and the hydrographic stations closer ~6 km. Averaged difference (Avg.) for all depths (black) and at 500 m depth (blue) is depicted. (c) Histogram of % of data points per difference between the gridded product and the hydrographic stations closer ~6 km for Θ at 0.1°C bins. (d) Mean squared error (MSE) between the gridded product and the hydrographic stations closer ~6 km for Θ. Inset shows the base 10 logarithmic scale in the x-axis.

https://doi.org/10.5194/essd-2020-244
Preprint. Discussion started: 23 September 2020

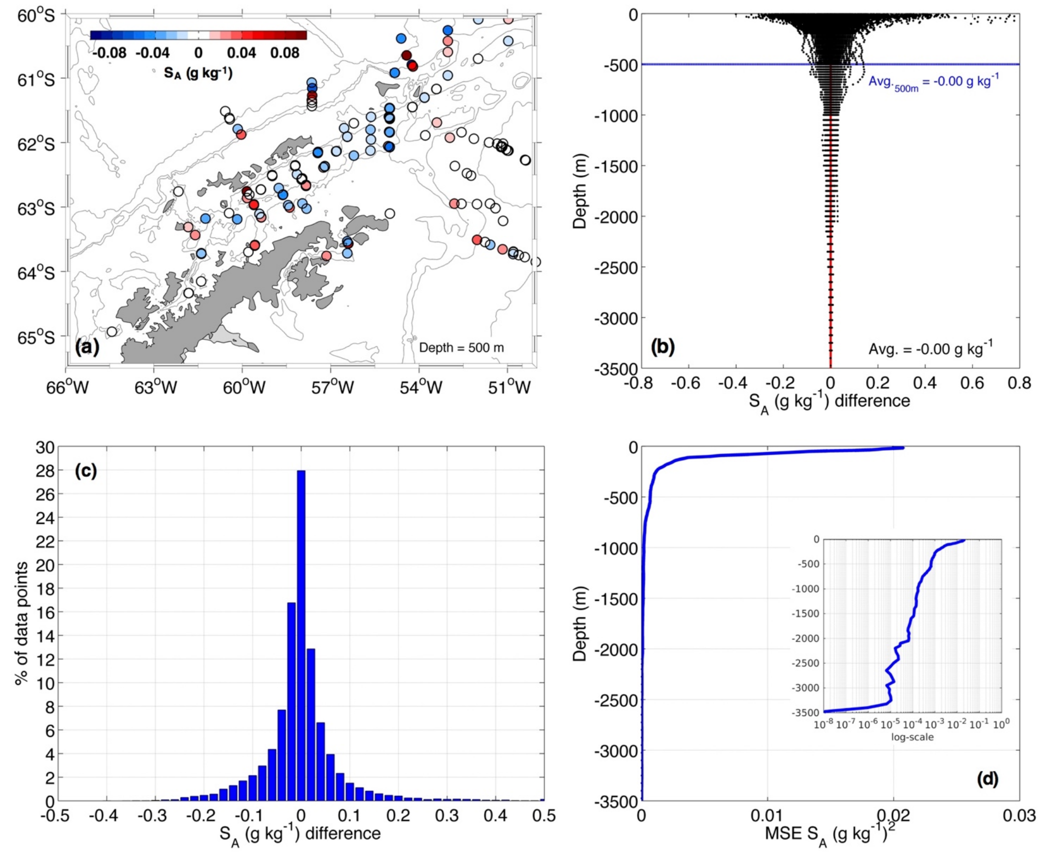

670

Figure 7. Same as Fig. 6, but for absolute salinity (S_A; g kg^{-1}). Note the range difference in the colorbar and the axes. In (c), the bins are 0.02 g kg^{-1}.

https://doi.org/10.5194/essd-2020-244
Preprint. Discussion started: 23 September 2020

Open Access Earth System Science Data Discussions

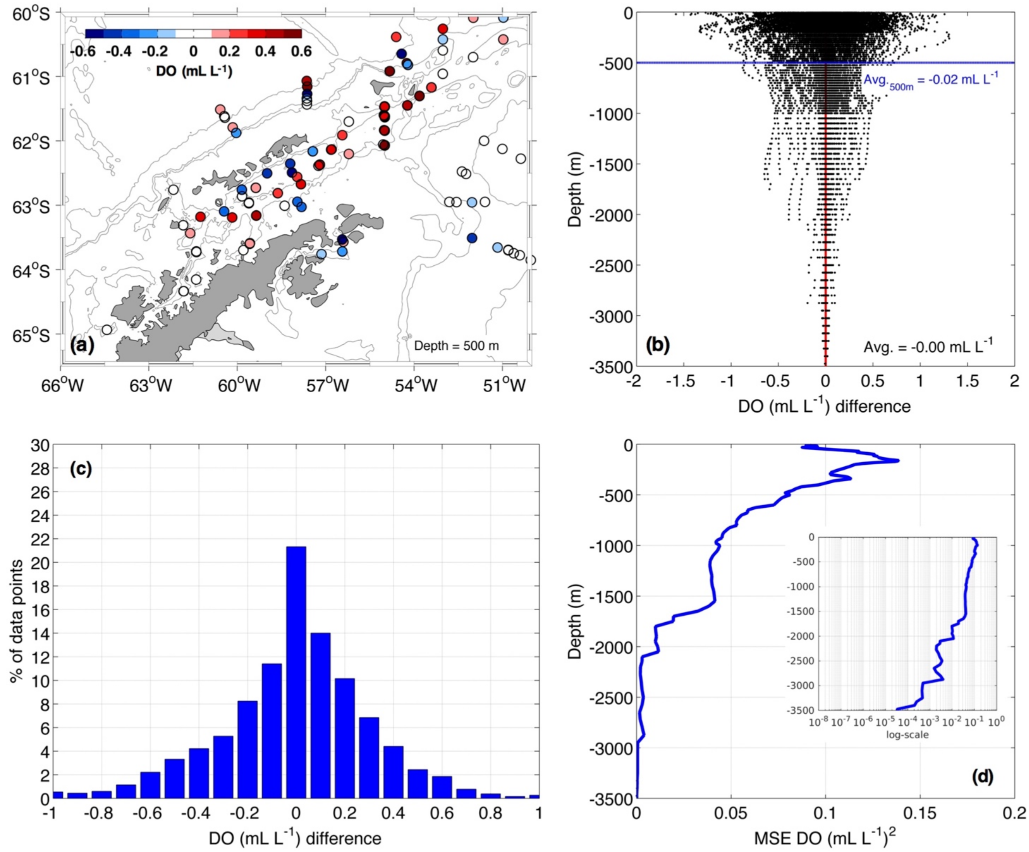

675

Figure 8. Same as Fig. 6, but for dissolved oxygen (DO; mL L^{-1}). In (c), the bins are 0.1 mL L^{-1}.

https://doi.org/10.5194/essd-2020-244
Preprint. Discussion started: 23 September 2020

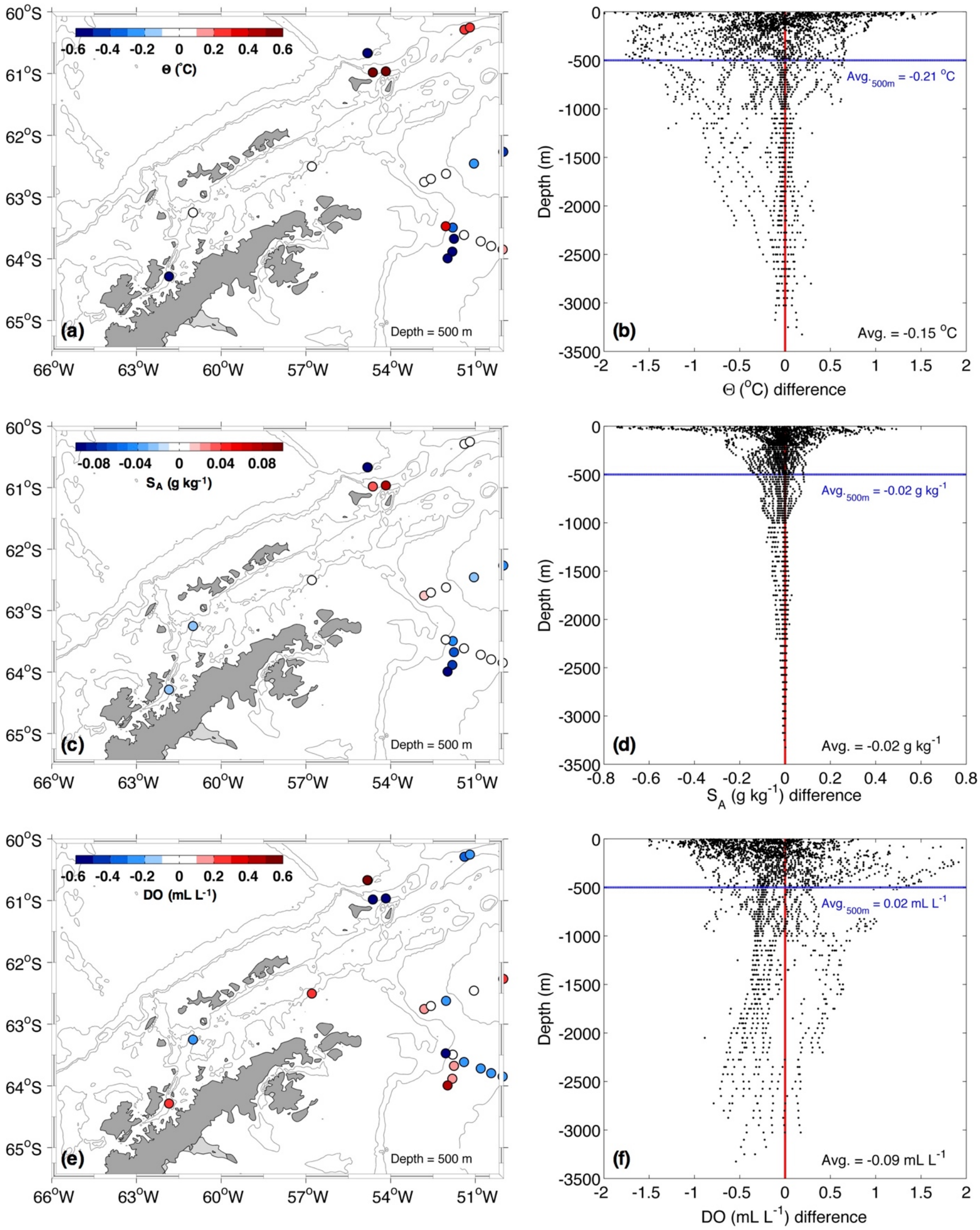

https://doi.org/10.5194/essd-2020-244
Preprint. Discussion started: 23 September 2020

Figure 9. Difference between the GOAL gridded product and the NODC hydrographic stations closer ~6 km at 500 m depth for (a) conservative temperature (Θ; °C), (c) absolute salinity (S_A; g kg^{-1}), and (e) dissolved oxygen (DO; mL L^{-1}). ETOPO1 isobaths of 500 m, 1000 m and 3000 m are depicted by black lines in (a), (c) and (e). Coastline from SCAR Antarctic Digital Database. Panels (b), (d) and (f) show the difference profile between the GOAL gridded product and the NODC hydrographic stations closer ~6 km for, respectively, Θ, S_A, and DO. Averaged difference (Avg.) for all depths (black) and at 500 m depth (blue) is depicted. NODC data were vertically interpolated into the standard depth levels (see Table 2).

https://doi.org/10.5194/essd-2020-244
Preprint. Discussion started: 23 September 2020

Open Access Earth System Science Data Discussions

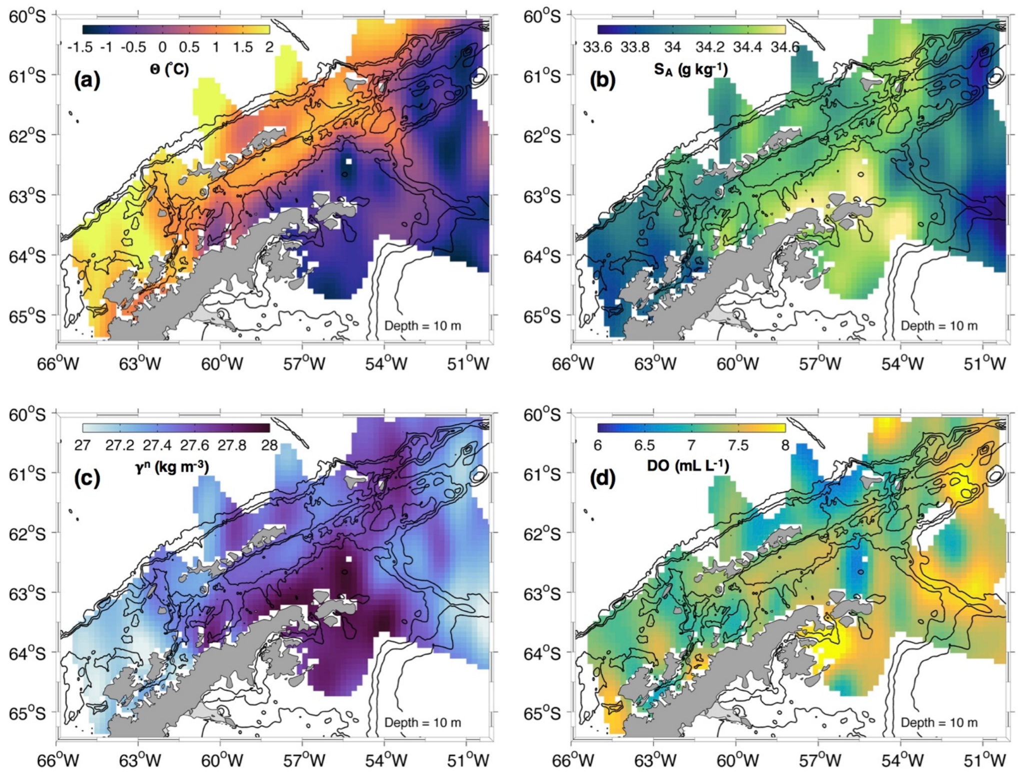

Figure 10. Surface maps of (a) conservative temperature (Θ; °C), (b) absolute salinity (SA, g kg^{-1}), (c) neutral density (γ^n; kg m^{-3}), and (d) dissolved oxygen (DO; mL L^{-1}) at 10 m depth based on GOAL gridded product. ETOPO1 isobaths of 500 m, 1000 m and 3000 m are depicted by the black lines. Coastline from SCAR Antarctic Digital Database.

690

https://doi.org/10.5194/essd-2020-244
Preprint. Discussion started: 23 September 2020

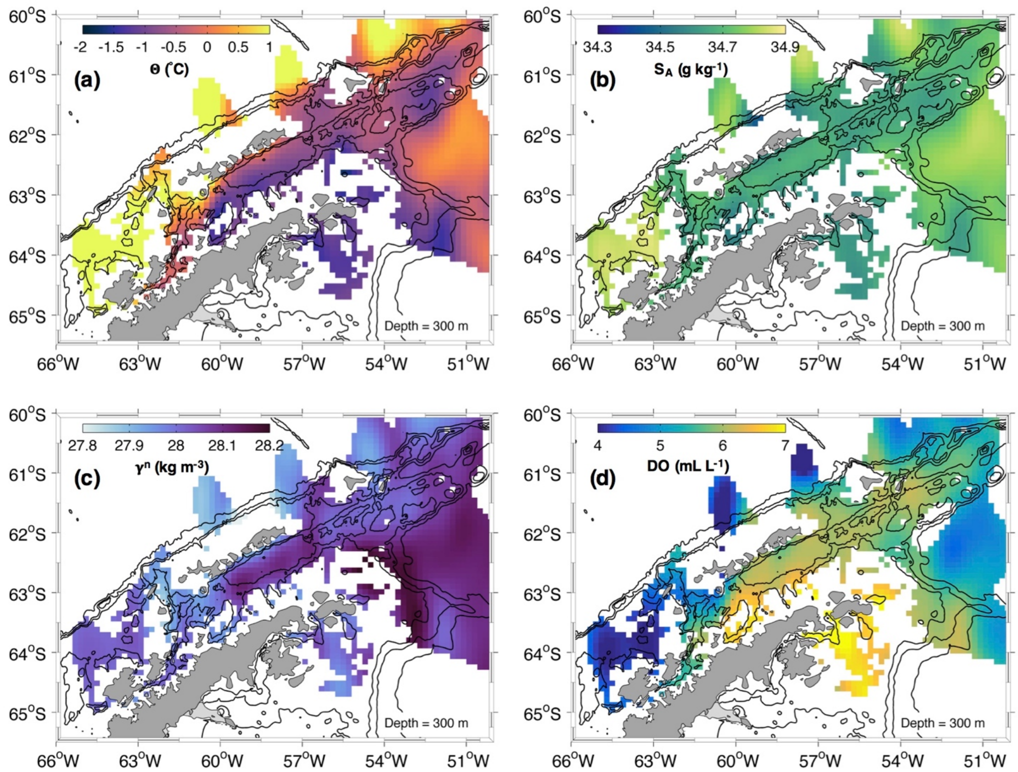

Figure 11. Same as Fig. 10, but for 300 m depth. Note the difference in the colorbar range.

https://doi.org/10.5194/essd-2020-244
Preprint. Discussion started: 23 September 2020

Open Access Earth System Science Data Discussions

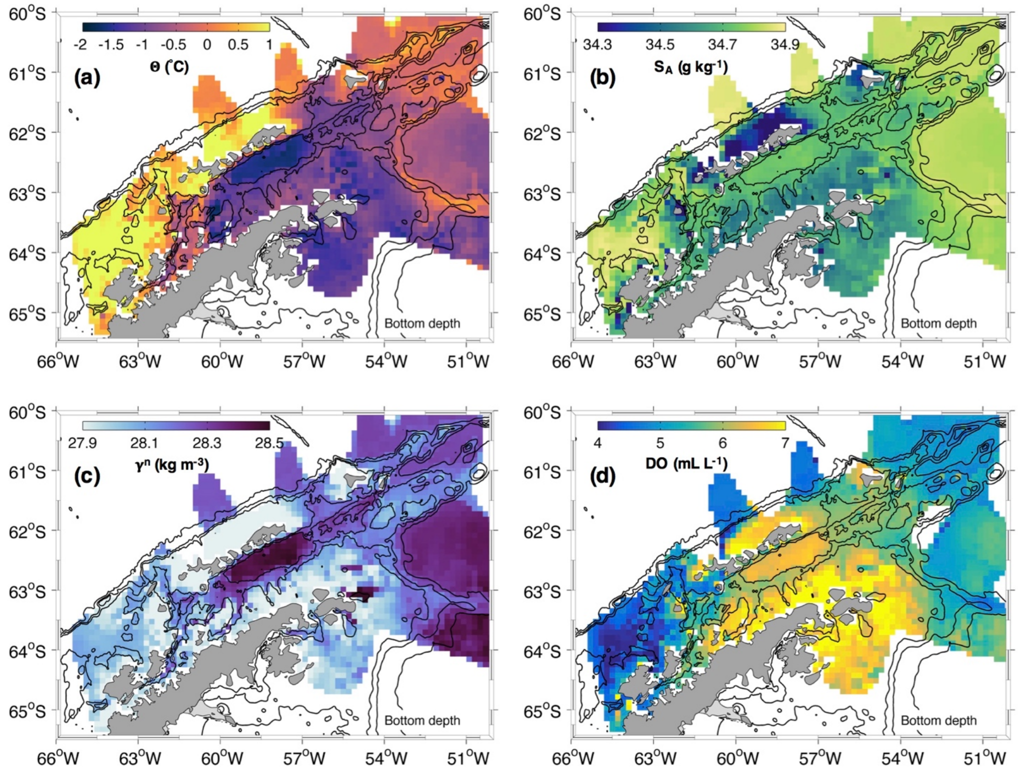

695 **Figure 12.** Same as Fig. 10, but for the pointwise bottom depth. Note the difference in the colorbar range.

https://doi.org/10.5194/essd-2020-244
Preprint. Discussion started: 23 September 2020

Open Access Earth System Science Data Discussions

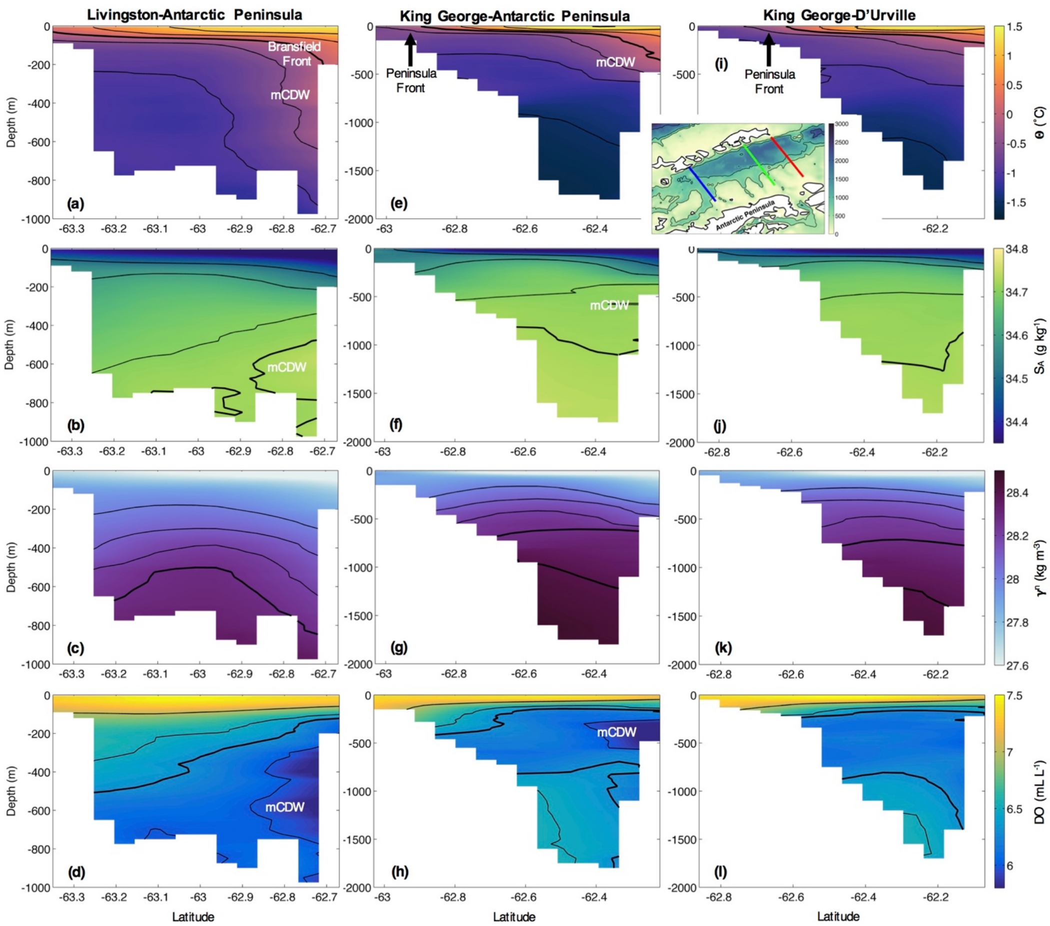

Figure 13. Vertical sections crossing the Bransfield Strait between the Livingston Island and the Antarctic Peninsula (a-d; blue line of the inset), King George Island and the Antarctic Peninsula (e-h; green line of the inset), and King George Island and the D'Urville Island (i-l; red line of the inset). Conservative temperature (Θ; °C) is shown in panels (a), (e) and (i). Isotherm of 0°C is shown by the thick black line. Thin lines show the isotherms of −1.5°C to +1.5°C every 0.5°C. Absolute salinity (S_A; g kg^{-1}) is shown in panels (b), (f) and (j). Isoline of 34.72 g kg^{-1} is shown by the thick black line. Thin lines show the isolines of 34.5 and 34.7 g kg^{-1} every 0.1 g kg^{-1}. Neutral density (γ^n; kg m^{-3}) is shown in panels (c), (g) and (k). The isolines of 28.27 and 28.40 kg m^{-3} are shown by the thick black lines. Thin lines show the isolines of 28.00 and 28.20 kg m^{-3} every 0.1 kg m^{-3}. Dissolved oxygen (DO; mL L^{-1}) is shown in panels (d), (h) and (l). The isolines of 6.3 mL L^{-1} is shown by the thick black lines. Thin lines show the isolines of 5.5 and 7.0 mL L^{-1} every 0.5 mL L^{-1}. Note the difference in the depth ranges. Inset shows the local bathymetry from ETOPO1 and the location of the sections. Coastline from SCAR Antarctic Digital Database.

https://doi.org/10.5194/essd-2020-244
Preprint. Discussion started: 23 September 2020

Open Access Earth System Science Data Discussions

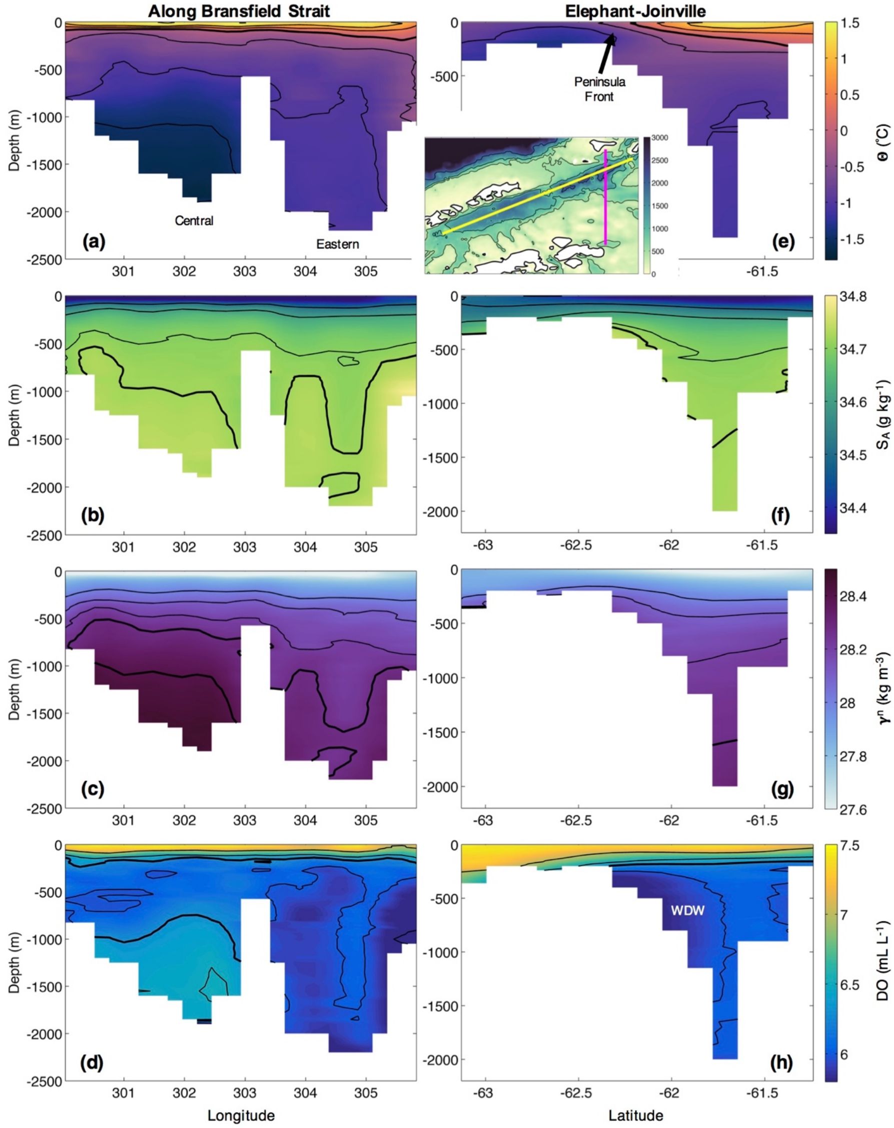

710 **Figure 14.** Vertical sections along the Bransfield Strait (a-d; yellow line of the inset) and between the Elephant Island and the Joinville Island (e-h; magenta line of the inset). Conservative temperature (Θ; ˚C) is shown in panels (a) and (e). Isotherm of 0˚C is shown by the thick black line. Thin lines show the isotherms of −1.5˚C to 1.5˚C every 0.5˚C. Absolute salinity (S_A; g kg^{-1}) is shown in panels (b) and (f). Isoline of 34.72 g kg^{-1} is shown by the thick black line. Thin lines show the isolines of 34.5 and 34.7 g kg^{-1} every 0.1 g kg^{-1}. Neutral density

https://doi.org/10.5194/essd-2020-244
Preprint. Discussion started: 23 September 2020

(γ^n; kg m^{-3}) is shown in panels (c) and (g). The isolines of 28.27 and 28.40 kg m^{-3} are shown by the thick black lines. Thin lines show the isolines of 28.00 and 28.20 kg m^{-3} every 0.1 kg m^{-3}. Dissolved oxygen (DO; mL L^{-1}) is shown in panels (d) and (h). The isolines of 6.3 mL L^{-1} is shown by the thick black lines. Thin lines show the isolines of 5.5 and 7.0 mL L^{-1} every 0.5 mL L^{-1}. Note the difference in the depth ranges. Bransfield Strait central and eastern basins are identified in panel (a). Inset shows the local bathymetry from ETOPO1 and the location of the sections. Coastline from SCAR Antarctic Digital Database.

https://doi.org/10.5194/essd-2020-244
Preprint. Discussion started: 23 September 2020

Open Access Earth System Science Data Discussions

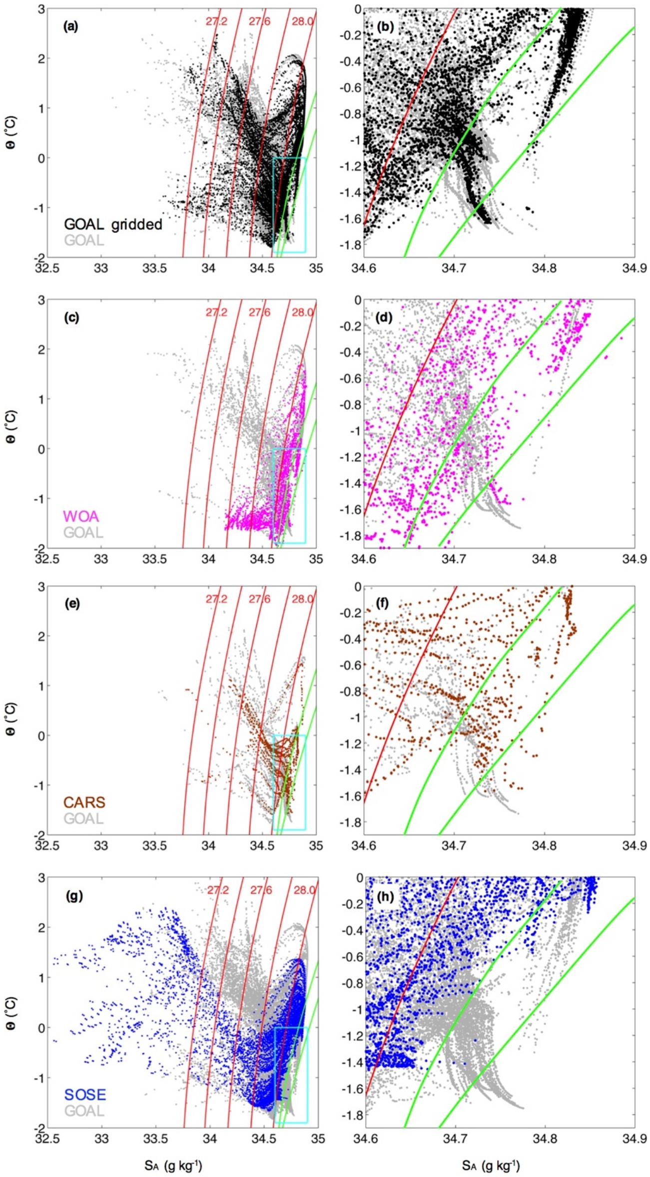

720

Figure 15. Conservative temperature-Absolute salinity (Θ-SA) diagrams for the different data set analysed: Brazilian High Latitude Group (GOAL), World Ocean Atlas (WOA), CSIRO Atlas of Regional Seas (CARS), Southern Ocean State Estimate (SOSE). Profiles collected

https://doi.org/10.5194/essd-2020-244
Preprint. Discussion started: 23 September 2020

by the GOAL and closer to ~6 km to the GOAL gridded products are shown in grey. (a and b) GOAL gridded product, (c and d) WOA, (e and f) CARS, and (g and h) SOSE. Neutral density isolines of 27.2 to 28.0 kg m^{-3} are shown every 0.2 kg m^{-3}. Green isolines depict 28.27 and 28.40 kg m^{-3} isopycnals. Cyan rectangles in (a), (c), (e) and (g) shows the dense water masses restriction presented in (b), (d), (f), and (h), respectively.

https://doi.org/10.5194/essd-2020-244
Preprint. Discussion started: 23 September 2020

Open Access Earth System Science Data Discussions

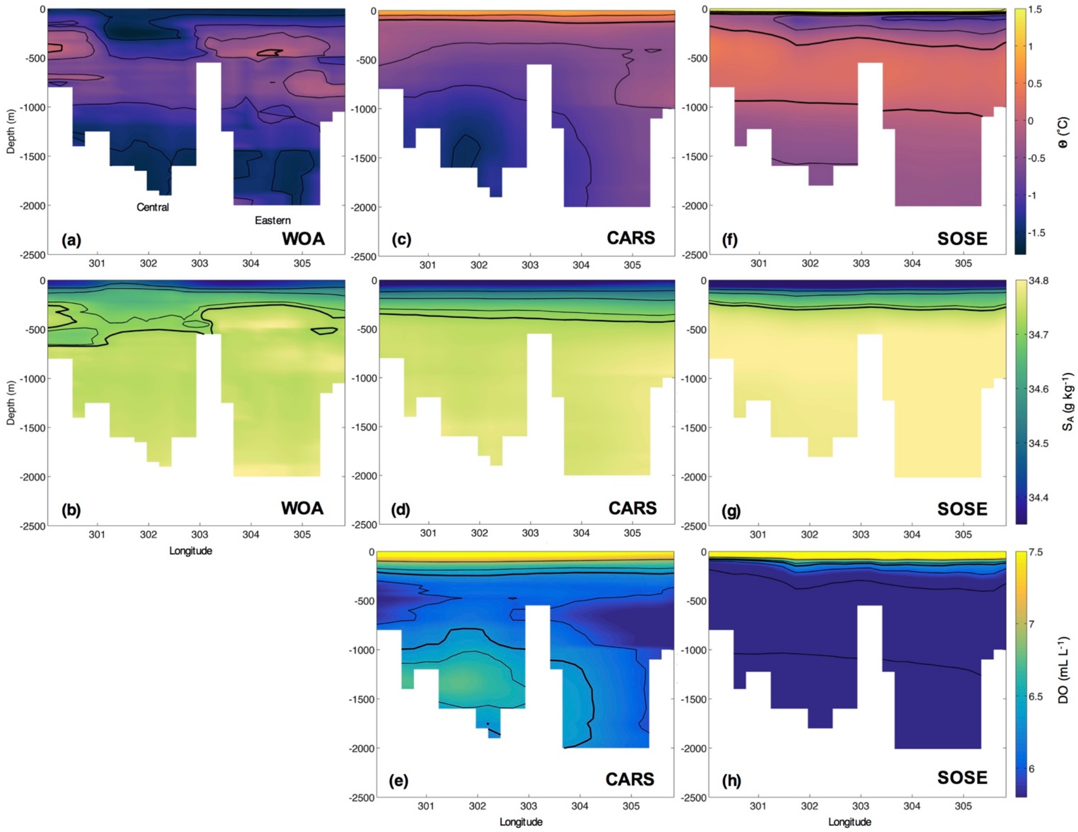

Figure 16. Vertical sections along the Bransfield Strait from World Ocean Atlas (WOA), CSIRO Atlas of Regional Seas (CARS), and
730 Southern Ocean State Estimate (SOSE). (a) WOA conservative temperature (Θ; °C). Isotherm of 0°C is shown by the thick black line. Thin lines show the isotherms of −1.5°C to 1.5°C every 0.5°C. Bransfield Strait central and eastern basins are identified in (a). (b) WOA absolute salinity (S_A; g kg^{-1}). Isoline of 34.72 g kg^{-1} is shown by the thick black line. Thin lines show the isolines of 34.5 and 34.7 g kg^{-1} every 0.1 g kg^{-1}. (c) Same as panel (a), but for CARS. (d) Same as panel (b), but for CARS. (e) CARS dissolved oxygen (DO; mL L^{-1}). The isolines of 6.3 mL L^{-1} is shown by the thick black lines. Thin lines show the isolines of 5.5 and 7.0 mL L^{-1} every 0.5 mL L^{-1}. (f) Same as panel (a), but
735 for SOSE. (g) Same as panel (b), but for SOSE. (h) Same as panel (e), but for SOSE.

https://doi.org/10.5194/essd-2020-244
Preprint. Discussion started: 23 September 2020

Open Access Earth System Science Data Discussions

Appendix A:

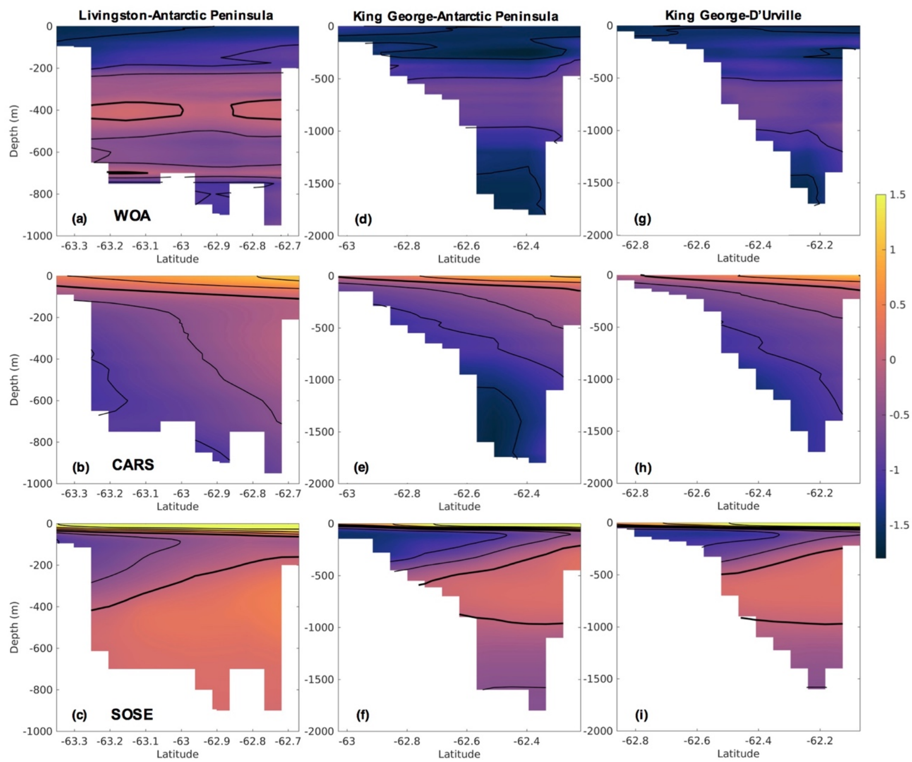

740 **Figure A1.** Vertical sections of crossing the Bransfield Strait between the Livingston Island and the Antarctic Peninsula (a-c), King George and the Antarctic Peninsula (d-f) and King George and D'Urville Island (g-i; see Fig. 13 for reference). Conservative temperature (Θ; °C) is shown for WOA (a, d and g), CARS (b, e and h), and SOSE (c, f and i). Isotherm of 0°C is shown by the thick black line. Thin lines show the isotherms of −1.5°C to 1.5°C every 0.5°C. Note the difference in the depth range.

https://doi.org/10.5194/essd-2020-244
Preprint. Discussion started: 23 September 2020

Earth System Science Data
Open Access
Discussions

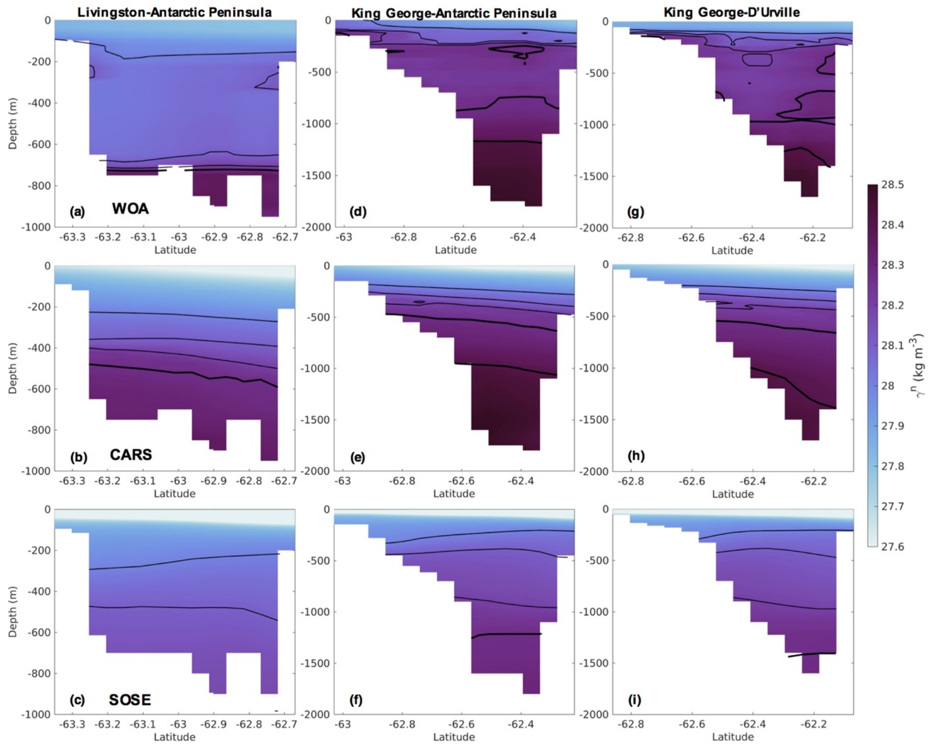

745 **Figure A2.** Vertical sections of crossing the Bransfield Strait between the Livingston Island and the Antarctic Peninsula (a-c), King George and the Antarctic Peninsula (d-f) and King George and D'Urville Island (g-i; see Fig. 13 for reference). Neutral density (γ^n; kg m^{-3}) is shown for WOA (a, d and g), CARS (b, e and h), and SOSE (c, f and i). The isolines of 28.27 and 28.40 kg m^{-3} are shown by the thick black lines. Thin lines show the isolines of 28.00 and 28.20 kg m^{-3} every 0.1 kg m^{-3}. Note the difference in the depth range.